SEDIMENTOLOGY the journal of the International Association of Sedimentologists

Sedimentology (2015) doi: 10.1111/sed.12220

Palaeoceanographic controls on spatial redox distribution over the Yangtze Platform during the Ediacaran–Cambrian transition

LAWRENCE M. OCH*, LORENZO CREMONESE*, GRAHAM A. SHIELDS-ZHOU*†, SIMON W. POULTON‡, ULRICH STRUCK§, HONGFEI LING¶, DA LI¶, XI CHEN¶, CHRISTINA MANNING**, MATTHEW THIRLWALL**, HARALD STRAUSS†† and MAOYAN ZHU†

**Department of Earth Sciences, University College London, Gower Street, London WC1E 6BT, UK (E-mail: lawrence.och@gmail.com)*

†State Key Laboratory of Palaeobiology and Stratigraphy, Nanjing Institute of Geology and Palaeontology, Chinese Academy of Sciences, Nanjing 21008, China

‡School of Earth and Environment, University of Leeds, Leeds LS2 9JT, UK

§Leibniz-Institut für Evolutions- und Biodiversitätsforschung, Museum für Naturkunde, 10115 Berlin, Germany

¶State Key Laboratory for Mineral Deposits Research, Department of Earth Sciences, Nanjing University, Nanjing 210093, China

***Department of Earth Sciences, Royal Holloway, University of London, Egham, Surrey TW20 0EX, UK*

††Institute for Geology and Paleontology, Westfälische Wilhelms-Universität Münster, 48149 Münster, Germany

Associate Editor – Ian Fairchild

ABSTRACT

The Ediacaran–Cambrian interval was an eventful transitional period, when dynamic interactions between the biosphere and its physical environment allowed the Earth System to cross into a new state, characterized by the presence of metazoans, more equable climates and more expansive oxygenation of the oceans. Due to the retreat of widespread sulphidic conditions, redox-sensitive trace-metals could accumulate to a greater extent in 'black shales' deposited in localized anoxic/euxinic environments, such as highly productive ocean margins. This study investigates the concentrations of the redox-sensitive trace-metals molybdenum and vanadium in organic-rich sedimentary rocks from seven sections of the Yangtze Platform, slope and basin. Iron speciation analyses were carried out in order to distinguish oxic, anoxic-ferruginous and anoxic-sulphidic settings, while sulphur and nitrogen isotope ratios were measured to gain insight into sulphate and nitrate availability, respectively, in the context of changing redox conditions. The data herein demonstrate an overall increase in redox-sensitive trace-metal contents in black shales across the Ediacaran–Cambrian transition, but with marked temporal and spatial variability. Euxinia is evident in South China before 551 Ma in the Ediacaran, and again in the early Cambrian. However, some time-equivalent sections are not enriched in redox-sensitive trace-metals, and also exhibit contrasting S-isotope and N-isotope systematics. A more complex configuration of the Yangtze Platform, for example with vast intra-shelf basins, together with changing (generally rising) eustatic sea-level may account for this variability. In this regard, it is proposed that a mid-depth sulphidic wedge, caused by nutrient upwelling over the south-east platform

margins, migrated over time (but generally landward), leading to spatially variable redox conditions determined by sea-level, currents and bathymetric constraints. The changing extents of anoxia and euxinia appear to have limited the distribution of emerging Ediacaran and Cambrian ecosystems.

Keywords Cambrian, Ediacaran, iron speciation, Neoproterozoic, nitrogen isotopes, redox-sensitive trace-metals, sulphide isotopes.

INTRODUCTION

Over its 4·6 billion year history, the Earth System evolved in several broad steps and experienced profound modifications, until a surface environment suitable for the diverse biosphere of today emerged after *ca* 4 billion years. Rarely, amid these seemingly slow and gradual changes, a threshold was crossed when major events followed in such quick succession that cause and effect relationships are difficult to distinguish. Such a 'revolution' happened during the Archean–Proterozoic transition when tectonic reconfigurations (Campbell & Allen, 2008; Reddy & Evans, 2009), major glaciations (Kirschvink *et al.*, 2000; Kasting & Ono, 2006), the emergence of eukaryotes (Brocks *et al.*, 1999; Knoll *et al.*, 2006) and a significant rise in atmospheric oxygen levels, termed the Great Oxidation Event (GOE) by Holland (2002), changed the face of the Earth. This first Oxygenation Event (e.g. Cloud, 1972; Holland, 1984, 2006; Des Marais *et al.*, 1992; Bekker *et al.*, 2004; Canfield, 2005) was originally believed to have led to at least moderate ventilation of the deep ocean, ending large-scale precipitation of banded iron formations *ca* 1·8 Ga (Holland, 1984, 2002; Isley & Abbott, 1999). Alternatively, Canfield (1998) proposed that the deep ocean developed widespread euxinia (anoxic-sulphidic water column conditions) after the GOE, because rising oxygen levels would have enhanced sulphate delivery to the ocean which then fuelled bacterial sulphate reduction (Canfield & Raiswell, 1999; Habicht *et al.*, 2002; Strauss, 2004). Widespread euxinia would, in turn, have resulted in titration of dissolved iron from the water column.

Such an anoxic and at least intermittently euxinic ocean after the GOE has been substantiated by several studies (Fig 1; Shen *et al.*, 2002, 2003; Arnold *et al.*, 2004; Poulton *et al.*, 2004; Brocks *et al.*, 2005; Sarkar *et al.*, 2010; Poulton & Canfield, 2011) and euxinia was probably an intermittent feature even across the Neoproterozoic–Cambrian boundary (Canfield *et al.*, 2008; Gill *et al.*, 2011). However, a growing body of evidence suggests that ocean redox gradients were more complex, with anoxic-sulphidic waters restricted to mid-water depths along productive continental margins, overlying anoxic-ferruginous deeper waters (Li *et al.*, 2010; Poulton *et al.*, 2010; Poulton & Canfield, 2011). A second oxidation event, termed the Neoproterozoic Oxygenation Event or NOE (Shields-Zhou & Och, 2011; Och & Shields-Zhou, 2012), may have occurred during the Neoproterozoic–Cambrian interval when, with a few notable exceptions (see Meyer & Kump, 2008, for a review), the deep ocean became pervasively oxygenated. The hypothesis of a NOE largely rests on several lines of geochemical evidence. Carbon isotope studies indicate that the fractional burial of reduced organic carbon was unusually high after *ca* 800 Ma (Des Marais *et al.*, 1992; Mills *et al.*, 2014). Although fractional burial estimates do not allow estimation of redox fluxes, higher proportional burial would most probably have resulted in atmospheric oxygenation during periods of enhanced chemical weathering, for example during the Ediacaran Period following the Cryogenian glaciations (e.g. Derry *et al.*, 1992). Apart from low stratigraphic resolution chromium isotope studies (Frei *et al.*, 2009), most other relevant geochemical data relate to changes in ocean redox and, in particular, a 'ventilation' of the deeper ocean realms during the Ediacaran Period (Canfield & Teske, 1996; Johnston *et al.*, 2005; Le Guerroué *et al.*, 2006; Canfield *et al.*, 2007, 2008; Scott *et al.*, 2008; Sahoo *et al.*, 2012). For example, Sahoo *et al.* (2012) used high levels of Mo enrichment in marine sediments deposited under anoxic conditions to demonstrate ocean (and possibly atmospheric) oxygenation in the wake of the end-Cryogenian 'Marinoan' glaciations at *ca* 632 Ma (Fig. 1). Algeo & Lyons (2006) have shown that Mo/TOC (total organic carbon) ratios probably represent a better proxy for the actual Mo budget in marine basins, and applying this ratio still shows an increase of at least one order of

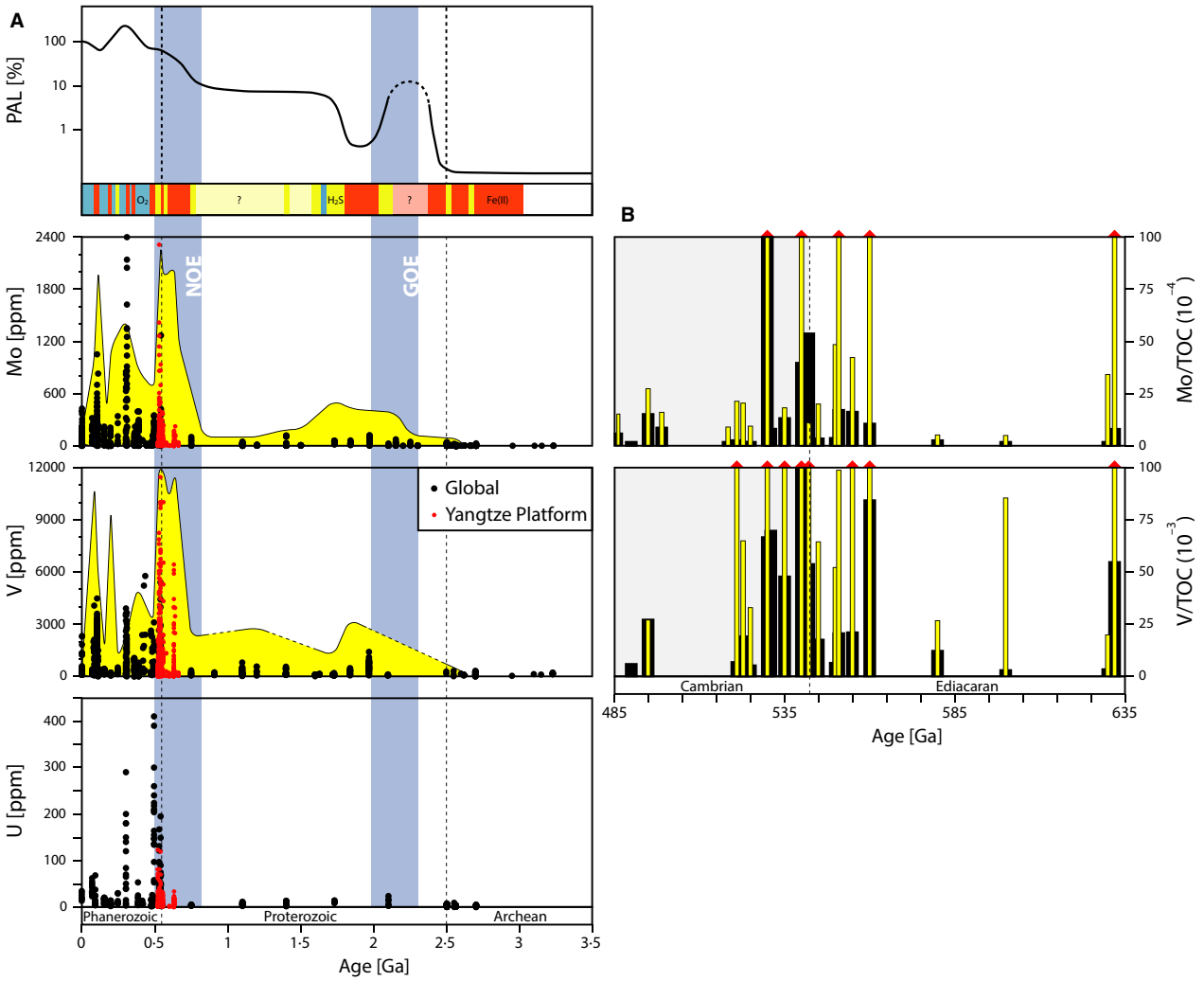

Fig. 1. (A) An attempt to illustrate the atmospheric oxygen level throughout the last 4 billion years (modified after Canfield, 2005) with concomitant changes in deep ocean redox conditions whereby anoxic-ferruginous (red) and euxinic (yellow) conditions prevail during the Precambrian before a dominantly oxygenated (blue) ocean characterizes the Phanerozoic (major uncertainty is shaded lightly and marked by a question mark; modified after Lyons & Gill, 2010, and extended after Shen *et al.*, 2002, 2003; Arnold *et al.*, 2004; Poulton *et al.*, 2004; Brocks *et al.*, 2005; Canfield *et al.*, 2008; Meyer & Kump, 2008; Reinhard *et al.*, 2009; Scott *et al.*, 2011; Partin *et al.*, 2013). Compilations of the redox-sensitive trace-metals Mo, V and U contents in anoxic, organic-rich sediments is shown below (filled circles) with the data collected from samples on the Yangtze Platform depicted in red (mostly from the present study but also from Wallis, 2006; Guo *et al.*, 2007; Scott *et al.*, 2008; Sahoo *et al.*, 2012). The Mo/TOC and V/TOC ratios, illustrated by the yellow shaded envelope, further indicate a major increase in the ocean trace-metal budget during and after both oxygenation events but, in particular, during the Neoproterozoic–Cambrian interval. A few ratios exceed the upper limit shown here and are likely to represent artefacts due to very low TOC (see Table S1). (B) Same dataset as in (A) but only for the Ediacaran and Cambrian period. The thick black bars represent the range of absolute Mo and V concentrations, while the thin grey bars show the range of Mo/TOC and V/TOC ratios. The red arrowheads indicate where Mo/TOC and V/TOC ratios exceed the depicted scale.

magnitude during the Ediacaran–Cambrian transitional interval (Fig. 1; Scott *et al.*, 2008; Sahoo *et al.*, 2012). A similar pattern is observed for other redox-sensitive trace-metals that are influenced minimally by detrital sources, such as vanadium and uranium (Fig. 1; Tribovillard *et al.*, 2006; Och & Shields-Zhou, 2012; Sahoo *et al.*, 2012; Partin *et al.*, 2013).

Due to predictable differences between the behaviour of different palaeoredox proxies under particular redox conditions, the use of a multiproxy approach is crucial to obtain a more

complete picture of the NOE. This is especially true considering that past ocean and atmospheric composition is difficult to quantify directly, while trace-metal budgets may have been significantly different from those of the modern ocean (Fig. 1; Scott *et al.*, 2008). In the present study a multiproxy approach has been applied involving trace element (Mo and V) concentrations, Fe speciation and stable isotopes ($\delta^{14}N$ and $\delta^{34}S$), to investigate redox variability, and controls on such variability, across the Yangtze Platform, slope and basin during the Ediacaran–Cambrian transition. The well-preserved organic-rich sedimentary successions on the Yangtze Platform offer an excellent opportunity to study changes in biogeochemical cycling during the Ediacaran–Cambrian transition. Some of the earliest and best preserved Ediacaran and Cambrian fossil assemblages are found on the Yangtze Platform, whereby phosphatized, possible animal embryos from the Ediacaran Doushantuo Formation (Xiao & Knoll, 2000), and the Early Cambrian Chengjiang Fauna, one of the earliest Burgess-shale type fossil occurrences (e.g. Babcock *et al.*, 2001; Hagadorn, 2002), are among the most intensely studied. Redox geochemistry during the putative NOE has mainly been inferred from single sedimentary successions deposited on the Yangtze Platform (Canfield *et al.*, 2008; Scott *et al.*, 2008; Sahoo *et al.*, 2012), while a relatively simple palaeobathymetry has been assumed in multiproxy palaeoredox studies (e.g. Li *et al.*, 2010; see also Cui *et al.*, 2015, for a critical re-evaluation). The present study aims to consolidate previously documented changes in redox geochemistry, with estimates of redox reservoir sizes based on S isotopes, and nutrient/redox dynamics inferred from N isotopes and Fe speciation. Furthermore, this multi-proxy approach is used to shed light on the complex inter-relationships between biogeochemical cycling and the broad morphological and bathymetric changes that occurred on the Yangtze Platform during the Ediacaran–Cambrian transition.

GEOCHEMICAL PROXIES

Redox-sensitive trace elements

Molybdenum is present as molybdate (MoO_4^{2-}; Broecker & Peng, 1982) in oxic sea water and is readily sequestered by Mn/Fe-oxyhydroxides and subsequently released to pore waters under reducing conditions (Crusius *et al.*, 1996; Goldberg *et al.*, 2012). In the presence of free H_2S (beyond a threshold concentration of *ca* 11 μM), molybdate can be converted to particle-reactive thiomolybdate ions (MoO_xS_{4-x}; Helz *et al.*, 1996; Erickson & Helz, 2000) and subsequently scavenged by metal-rich particles, sulphur-rich organic molecules (Helz *et al.*, 1996, 2011; Tribovillard *et al.*, 2004) and iron sulphide minerals (Vorlicek *et al.*, 2004; Poulson Brucker *et al.*, 2012). In the modern ocean, oxic–suboxic facies represent the most important sink for Mo but, despite only making up *ca* 0·3% of the sea floor, euxinic environments account for *ca* 30 to 50% of Mo removal from the water column (Bertine & Turekian, 1973; Morford & Emerson, 1999; Anbar, 2004; Algeo & Lyons, 2006), illustrating that Mo is mainly enriched in deposited sediments under sulphidic conditions (e.g. Piper, 1994; Tribovillard *et al.*, 2006).

In oxic sea water, vanadium is present as vanadate oxyanions (HVO_4^{2-} and $H_2VO_4^-$) and readily adsorbs onto both Mn-oxyhydroxides and Fe-oxyhydroxides (Calvert & Piper, 1984; Wehrli & Stumm, 1989) and possibly kaolinite (Breit & Wanty, 1991). Mildly reducing conditions lead to the formation of vanadyl ions (VO^{2-}), related hydroxyl species ($VO(OH)_3^-$) and insoluble hydroxides $VO(OH)_2$. More strongly reducing conditions can lead V to be taken up by geoporphyrins or precipitated as solid oxide (V_2O_3) or hydroxide ($V(OH)_3$) (Breit & Wanty, 1991; Wanty & Goldhaber, 1992). In general, sedimentary V enrichment begins under denitrifying conditions (e.g. Piper, 1994; Tribovillard *et al.*, 2006), making it more sensitive to less extreme redox conditions than Mo.

Although Mo and V are not dominantly delivered to the sediment in association with organic matter, concentrations often track TOC in anoxic non-sulphidic environments. However, under euxinic conditions, concentrations tend to be decoupled from TOC, resulting in higher Mo/TOC and V/TOC ratios (Tribovillard *et al.*, 2006, and references therein). Molybdenum and, in a less efficient way, V also represent key bio-nutrients which are mainly involved in nitrogenase, an enzyme used in nitrogen-fixing bacteria (Stiefel, 1997; Anbar & Knoll, 2002; Eady, 2003; Zerkle *et al.*, 2006; Canfield *et al.*, 2010b). It has been hypothesized that such trace-metals might have been the limiting nutrients in the Precambrian ocean, as opposed to phosphorus during the Phanerozoic (Anbar & Knoll, 2002; Planavsky *et al.*, 2010;

Zhang *et al.*, 2014; see also Godfrey *et al.*, 2013). Today, however, the budgets of Mo and V are not controlled by marine plankton, i.e. by their roles as micronutrients (e.g. Ho *et al.*, 2003; Tribovillard *et al.*, 2006), and Mo does not exhibit a nutrient-like distribution (concentrations remain relatively constant through the water column), while V exhibits only minor depletion in the photic zone (Collier & Edmond, 1984; Collier, 1985; Piper, 1994).

A complication with the use of Mo-based redox proxies is that the importance of euxinia on a global scale is often assessed from the level of Mo enrichment (or Mo isotope value) in euxinic black shales on a local scale (e.g. Scott *et al.*, 2008). Local Mo enrichment in black shales is generally taken to indicate a lack of Mo sequestration on a global scale, while low Mo concentrations are taken to indicate that the global ocean Mo reservoir has been reduced due to widespread Mo sequestration. However, the absolute level of Mo-enrichment may also reflect the degree of euxinia, or other factors such as basin restriction or sedimentation rate. Therefore, for Mo to be an effective predictor of global euxinia, local redox conditions must be established using independent means, such as Fe speciation, while the nature of the basin and sedimentation characteristics need to be considered.

Iron speciation

Iron speciation analyses of marine sediments are increasingly being used to infer the redox conditions that prevailed in the water column above a depositional environment; for example in modern (Canfield *et al.*, 1996; Raiswell & Canfield, 1996, 1998), Phanerozoic (Raiswell *et al.*, 2001; Poulton & Raiswell, 2002), Proterozoic (Shen *et al.*, 2002, 2003; Poulton *et al.*, 2004, 2010; Canfield *et al.*, 2007, 2008; Sahoo *et al.*, 2012) and Archean (Reinhard *et al.*, 2009; Kendall *et al.*, 2010) settings. The Fe speciation scheme identifies several operationally derived iron pools (Poulton & Canfield, 2005), whereby iron species are characterized as either being unreactive (mostly silicate Fe) or highly reactive towards dissolved sulphide (Fe_{HR}). Highly reactive Fe includes four pools, namely pyrite Fe (Fe_{py}), magnetite Fe (Fe_{mag}), reducible-oxide Fe (Fe_{ox}) and carbonate-associated Fe (Fe_{carb}). The Fe_{Py}/Fe_{HR} ratio must be applied in combination with the Fe_{HR}/Fe_T ratio in order to determine whether the deposition of a given marine sediment occurred under oxic, anoxic-ferruginous or anoxic-sulphidic conditions. In modern marine sediments deposited under an oxic water column, the Fe_{HR}/Fe_T ratio does not exceed 0·38 (Raiswell & Canfield, 1998; Canfield *et al.*, 2008; Poulton & Canfield, 2011). A higher proportion of highly reactive iron would indicate an anoxic water column and, for these samples, the Fe_{Py}/Fe_{HR} ratio separates ferruginous (<0·8) from sulphidic (>0·8) bottom waters. Ratios between 0·7 and 0·8, however, are equivocal and do not necessarily exclude sulphidic conditions (März *et al.*, 2008; Poulton & Canfield, 2011).

Stable isotopes

The removal of sulphur from the ocean is controlled by pyrite formation (which is often accompanied by a large isotopic fractionation), and the precipitation of evaporites (accompanied by negligible fractionations (e.g. Canfield, 2001). Today, the most important catalyst for sulphur isotope fractionation is the sulphur metabolism of microbes, especially during, but not restricted to, the process of sulphate reduction (Jones & Starkey, 1957; Harrison & Thode, 1958; Kaplan & Rittenberg, 1964) which has been active since the Archean (Shen *et al.*, 2001; Shen & Buick, 2004; Archer & Vance, 2006). The following major controls on isotope fractionation during sulphate reduction can be formulated (Canfield, 2001): (i) when organic electron donors are used, lower specific rates of sulphate reduction lead to higher fractionations; (ii) lower fractionations (3 to 16‰; Kaplan & Rittenberg, 1964; Kemp & Thode, 1968) are achieved when H_2 is used as electron donor, particularly at low specific rates of sulphate reduction; (iii) small fractionations (<4‰) occur under sulphate-limiting conditions (*ca* 200 μM, e.g. Habicht *et al.*, 2002); and (iv) high fractionations reaching up to 70‰ occur when sulphate is more abundant (>1 mM; Canfield & Teske, 1996; Canfield *et al.*, 2010a). Controls (iii) and (iv) are commonly used to estimate marine sulphate concentrations.

The stable isotope signature of nitrogen, $\delta^{15}N$, can potentially give additional insights into the prevailing redox conditions in the water column, as well as the biochemical reactions involving nitrogen (Quan & Falkowski, 2009; Sigman *et al.*, 2009; Boyle *et al.*, 2013; Quan *et al.*, 2013; Ader *et al.*, 2014). Among all water column nitrogen reactions, incomplete denitrification gives the highest positive isotope frac-

tionation, leaving the residual nitrate pool enriched in ^{15}N, which is subsequently utilized by autotrophs to produce ^{15}N-enriched organic matter (Sigman *et al.*, 2009). Denitrification occurs at the suboxic/oxic boundary in the water column, and its intensity depends on the size of the nitrate pool and oxidative conditions. On the other hand, N_2 fixation by Mo-nitrogenase is carried out by diazotrophic cyanobacteria transferring atmospheric nitrogen into the oceanic pool, whereby the $\delta^{15}N$ of newly fixed N is *ca* −1‰ (e.g. Zhang *et al.*, 2014). Furthermore, as shown in a recent study by Zhang *et al.* (2014), the $\delta^{15}N$ value resulting from nitrogen fixation by alternative (i.e. the V-only and Fe-only) nitrogenases can lead to significantly lower $\delta^{15}N$ values (below −2‰). Generally speaking, vigorous denitrification will increase the nitrogen pool isotopic signature, while intense nitrogen fixation (for example, in the case of sea water nitrogen depletion) will stabilize values at *ca* 0‰. For these reasons, under anoxic conditions nitrification (and thus denitrification) is inhibited, while under euxinic conditions, including in the photic zone, N_2 fixation becomes more highly favoured. In the latter scenario, nitrogen isotopic values can be negative (Higgins *et al.*, 2012; Johnston *et al.*, 2009; Meyers *et al.*, 2012; Struck, 2012; Godfrey *et al.*, 2013). In addition, higher $\delta^{15}N$ values in well-preserved sediments can indicate the transition between anoxic and oxic conditions (in both directions), while lower values suggest either an oxic or anoxic environment (Quan *et al.*, 2008). Because denitrification during early diagenesis does not lead to significant isotopic fractionation in comparison to water column denitrification (Brandes & Devol, 2002), the $\delta^{15}N$ signature can be a reliable redox proxy when used in combination with independent measures, such as the redox-sensitive trace-metals Mo and V described above. The present study discusses published $\delta^{15}N$ profiles within this wider redox context (Cremonese *et al.*, 2013, 2014). In addition, it has been hypothesized that euxinic conditions, evidenced by high Mo/TOC and high Fe_{Py}/Fe_{HR} ratios, will affect the nitrogen isotope composition of organic matter in a systematic way, lowering $\delta^{15}N$ to atmospheric values (Boyle *et al.*, 2013). However, this idea can only be tested properly in integrated geochemical studies (e.g. Godfrey *et al.*, 2013).

GEOLOGICAL SETTING

The broader tectonic context

The Neoproterozoic sedimentary successions of the Yangtze Platform were greatly influenced by the tectonic history of the South China craton, one of three major tectonic cratons in China (Fig. 2). The South China craton consists of the Yangtze and Cathaysia blocks, which amalgamated during the Sibao–Jinning orogeny at *ca* 900 Ma (Li *et al.*, 1995, 2002, 2003b, 2005). During the break-up of Rodinia, whereby a plume-centre was possibly located under South China, inducing widespread granite intrusions (such as the 819 ± 7 Ma Huangling Granite in the Three Gorges Area) around the Yangtze block (Li *et al.*, 1999, 2003a), major rift basins formed along the south-eastern and western margins of the South China craton (Li *et al.*, 2003b; Wang & Li, 2003). The subsequent thermal subsidence created the necessary accommodation space for the Cryogenian–Silurian sediments that unconformably overlie Mesoproterozoic metamorphic rocks or early Neoproterozoic rift-related bimodal magmatic rocks, reflecting the different rifting phases (Wang & Li, 2003). The Yangtze Platform can be described schematically as comprising a large platformal area, transitioning into a slope and basin (Fig. 2). However, more precise palaeobathymetric reconstructions have shown that a generally shallow-water platform was characterized by numerous intra-shelf basins and carbonate barriers on its margins (Zhu *et al.*,

Fig. 2. Simplified geological map of South China with the locations of the studied sections in both, the Yangtze Platform and the basin (modified after Steiner *et al.*, 2001; Ling *et al.*, 2007) with a simplified stratigraphic overview of the Yangtze Platform (modified after Jiang *et al.*, 2007). The smaller scale map shows the geological map of the Three Gorges Area (modified after McFadden *et al.*, 2008) with a more detailed stratigraphy of the Precambrian–Cambrian transition. The pink shaded sections indicate occurrences of the main black shale successions. The yellow dots on both maps indicate the sections analysed for the present study whereas the Baiguoyuan section (white dot) has been considered from earlier analysis (Wallis, 2006). Localities investigated during recent studies by Li *et al.* (2010) and Sahoo *et al.* (2012) have also been included for comparison. Shp = Shipai Formation; Cr = Cryogenian Period.

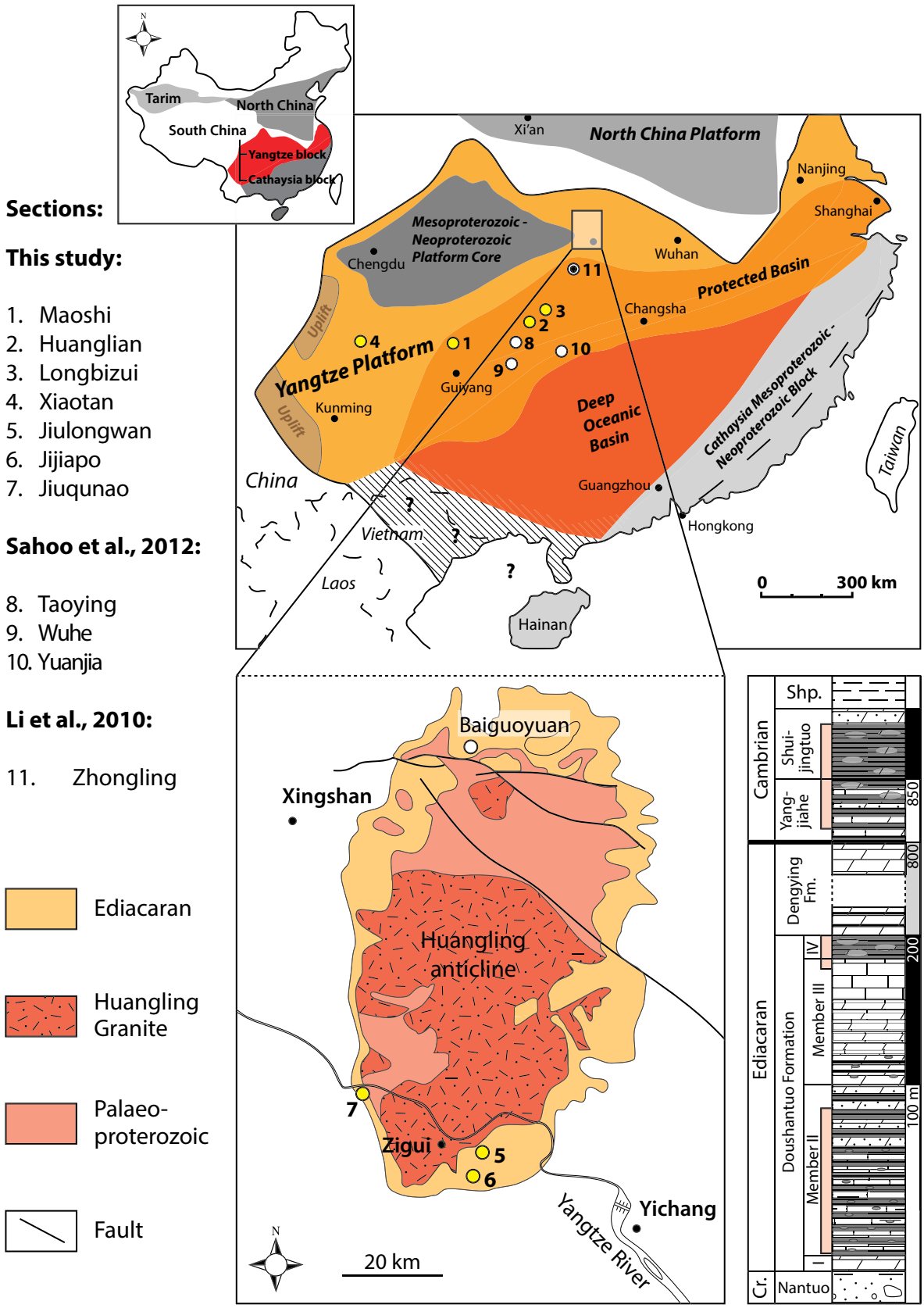

2003, 2007, 2013; Vernhet, 2007; Vernhet & Reijmer, 2010; Jiang *et al.*, 2011).

The Neoproterozoic sedimentary successions of the Yangtze Platform, which despite the complex tectonic history of China remained relatively undeformed, can be subdivided into three main intervals: pre-glacial predominantly volcano-siliciclastic rocks (for example, the *ca* 750 Ma Liantuo Formation on the platform and the approximately contemporaneous more fine-grained Banxi Group in the basin), two Cryogenian glacial diamictite intervals (the Gucheng/Tiesiao/Chang'an formations and Nantuo Formation, respectively) separated by an interglacial unit (the Datangpo/Xiangmeng formations) and post-glacial Ediacaran marine carbonates and shales (the Doushantuo Formation and the Dengying/Liuchapo formations). The Early Cambrian successions are found over both the platform and basin areas, characterized by black shales with abundant carbonate concretions overlying phosphatic strata of the lowermost Cambrian; they can be very condensed on the platform margin and very thick on the platform (Och *et al.*, 2013), in particular in the south-west (Yunnan & Guizhou provinces).

The Doushantuo Formation

The Doushantuo Formation is among the most extensively studied Neoproterozoic formations worldwide, notably because it accommodates the richest fossil record of this crucial time period, including acritarchs, multicellular algae and controversial fossil embryos (Xiao *et al.*, 1998; Zhang *et al.*, 1998; Xiao & Knoll, 2000; Condon *et al.*, 2005; Jiang *et al.*, 2006; Ling *et al.*, 2007; Yin *et al.*, 2007; McFadden, 2008; McFadden *et al.*, 2008; Ohno *et al.*, 2008; Lu *et al.*, 2013; Zhu *et al.*, 2013). Overlying the glacial diamictites of the Nantuo Formation, the basal Ediacaran cap carbonate of the Doushantuo Formation represents the aftermath of the end-Cryogenian 'Snowball Earth' glaciation (Hoffman *et al.*, 1998). Based on U–Pb age constraints (Condon *et al.*, 2005) and an extremely negative $\delta^{13}C$ excursion of arguable duration between *ca* 565 Ma and 550 Ma, the upper Doushantuo Formation has been correlated with the Johnnie Formation of Death Valley (USA), the Wonoka Formation of the Adelaide rift complex (Australia), the Shuram Formation in Oman, the post-Marinoan Windermere Supergroup (Canada), the Nama and Tsumeb groups of Namibia and south-east Siberia (Le Guerroué *et al.*, 2006; Zhou & Xiao, 2007; Lu *et al.*, 2013).

Although the Doushantuo Formation was deposited over the time span from 635 to 551 Ma (i.e. encompassing *ca* 90% of the Ediacaran Period; Condon *et al.*, 2005), it nowhere exceeds a thickness of *ca* 320 m. Whether this reflects a condensed succession or major undetected breaks in sedimentation is presently unclear, although the former possibility is favoured (Zhou *et al.*, 2007). Vernhet (2007) identified three different depositional environments in a study of several sections in Hunan, Guizhou and Hubei provinces, spanning the shallow, subtidal shelf environment, through intertidal or shoal settings, to deep-water basinal environments, illustrating the wide bathymetric range under which sedimentation of the Doushantuo Formation took place on the Yangtze Platform. Two and a half stratigraphic sequences (i.e. transgressive–regressive cycles), have been identified (Zhu *et al.*, 2007, 2013; McFadden *et al.*, 2008); they are, however, clearest in the shallower water facies and not easily discernible in the Yangtze Gorges Area (Zhu *et al.*, 2013).

In the Yangtze Gorges Area, the type locality of the Ediacaran System (known as the Sinian in China), the Doushantuo Formation can be subdivided into four lithological members (Wang *et al.*, 1998). Member I consists of a succession of cap carbonates (dolostone) which extend throughout the central and southern Yangtze Platform; they are characterized by tepee-like structures, sheet cracks, macropeloids, barite crystal fans and negative $\delta^{13}C$ values (Jiang *et al.*, 2003a, 2006; Zhou *et al.*, 2004). A precise U–Pb age of $635{\cdot}2 \pm 0{\cdot}6$ Ma has been determined from an ash layer within the cap carbonate at one locality (Condon *et al.*, 2005). In the Three Gorges Area, the cap carbonates have a thickness of *ca* 5 m and are thus relatively thin compared to some basal Ediacaran cap carbonates around the world (Hoffman *et al.*, 2007). The overlying second member is between 80 m and 140 m thick and is composed of interbedded black shale, organic-rich calcareous mudstone and thinly bedded dolomicrite. An ash layer dating from $632{\cdot}5 \pm 0{\cdot}5$ Ma is situated a few metres above the cap carbonate (Condon *et al.*, 2005). Abundant centimetre-sized chert nodules, decreasing up-section, occur in the lower–middle part of Member II and contain numerous acanthomorphic acritarchs and multicellular algae (Zhang *et al.*, 1998; Yin *et al.*,

2007; Zhou *et al.*, 2007). The sparse sedimentary structures include parallel laminations, crinkle laminations and rare intraformational breccias, indicating that wave and current activity were mostly absent during sedimentation of member II (Zhou *et al.*, 2007). This is likely to have resulted from the Yangtze Gorges Area being: (i) a protected basin; and/or (ii) overlain by a water depth exceeding *ca* 100 m (i.e. below 'storm-wave base'; Zhu *et al.*, 2013).

Member III is between 30 m and 60 m thick and comprises medium to thick-bedded dolostone with thin chert horizons and irregular chert nodules that grade up section into thin-bedded limestone and dolomitic interbeds (i.e. ribbonites). Although most chert layers are diagenetic in origin, some contain well-preserved microfossils (Zhang *et al.*, 1998; Xiao, 2004; Yin *et al.*, 2007). Sedimentary structures include scour marks, crinkle laminations and low angle cross-bedding, while sandy layers capping limestone and dolomite bedding surfaces are common, indicating that deposition occurred at shallower water depths than the underlying Member II, possibly in shallow subtidal environments (Zhou *et al.*, 2007). Member IV, commonly referred to as the Miaohe Member, comprises a succession of black shales and organic-rich mudstones. Sedimentary structures are absent apart from the fine lamination and abundant, sometimes huge (diameter >1 m), carbonate concretions of diagenetic origin (e.g. Lu *et al.*, 2013; Zhu *et al.*, 2013). Pyrite and barite are also common features of this member. An ash bed at the top of the Miaohe Member yields a U–Pb age of 551·1 ± 0·7 Ma, and a 3 to 4 cm thick bentonite bed that in some sections separates the Doushantuo Formation from the Dengying Formation has yielded an age of 550·4 ± 0·8 Ma (Condon *et al.*, 2005).

Studied sections

Black shale successions of the Doushantuo Formation were studied, predominantly from Members II and IV, at several locations on the Yangtze Platform: Jiulongwan (Jiulongwan and Xiangdangping) and Jiuqunao (Jijiawan) in the Yangtze Gorges Area, Hubei Province, and at Maoshi (north-west of Zunyi, Guizhou Province). At the Jiulongwan section, a substantial part of Member II was sampled from directly above the cap carbonate throughout a tectonically disrupted succession of massive grey dolomite beds with interbedded black shales. Further outcrops sampled at Jiulongwan comprise the >10 m thick Miaohe Member, consisting of laminated black shales, barite and abundant huge carbonate nodules which lie between Member III and the wavy, shaly horizon with a pyrite-rich layer that constitutes the contact to the overlying Dengying Formation Below the Miaohe Member, the top of Member III consists of dark grey dolomite which transitions downwards into paler carbonate ribbonites, followed by dolomite beds with some intercalated chert beds. The boundary between the Doushantuo Members II and III is obscured by poor outcrops and dense vegetation in this region.

At the Jiuqunao section, the lower black shales of the Doushantuo Member II and the black shales of the Miaohe (Doushantuo Member IV) have been investigated. Parts of Member III, particularly towards the top, consist of massive dolostone, which is considered to represent allochthonous blocks, due to either slumping and/or faulting (Lu *et al.*, 2013).

The upper Doushantuo Formation, including the transition to the overlying Dengying Formation was also sampled at the Maoshi section, Guizhou Province, where it was presumably deposited in a lagoonal setting close to the margin of the Yangtze Platform (e.g. Jiang *et al.*, 2011). Here, the upper Doushantou Formation is characterized by carbonate-rich black shales that can tentatively be correlated with the Miaohe Member (Doushantuo Member IV). The black shale unit at the top of the Doushantuo Formation occurs in almost all palaeoenvironments of the Yangtze Platform and its sharp onset represents a flooding surface (Jiang *et al.*, 2007) rather than a major sequence boundary (Zhu *et al.*, 2007, 2013). Similar to the cap carbonates, it can be used as a regional stratigraphic marker. However, due to lithostratigraphic variability within the Doushantuo Formation throughout South China, it is unclear to what extent the subdivision into four members can be applied away from the southern limb of the Huangling granite in the Yangtze Gorges Area (Zhu *et al.*, 2007, 2013).

The Dengying/Liuchapo formations

In contrast to the underlying Doushantuo Formation, a relatively short time interval, from *ca* 551 to 541 Ma, is represented by the Dengying Formation (Zhao *et al.*, 1988). In places, this formation is much thicker (240 to 850 m), and can be subdivided into three members. In the Three Gorges Area these are: (i) the Hamajing Member

at the base (20 to 190 m thick), consisting of light-grey, medium to thick-bedded dolomite with intercalated thin chert layers; (ii) the overlying Shibantan Member (100 to 160 m), characterized by dark grey, thin-bedded limestone; and (iii) the Baimatuo Member (60 to 570 m), which is composed of light-grey, thickly bedded/massive dolomite. The tripartite subdivision of the Dengying Formation can be recognized in many places in South China, although a different terminology is sometimes used (Ding *et al.*, 1992; Zhu *et al.*, 2003).

A few samples near the top of the Dengying Formation, just below the Early Cambrian successions, notably the Jijiapo (Hubei Province) section, were collected and analysed but, due to their trace-metal content close to detection limit, they will not be discussed in the present study (see Och, 2011, for details). At the Maoshi section, the lower part of the Dengying Formation comprises a succession of alternating black carbonates, which get paler up-section, and sandy carbonates. At the Jijiapo section, Three Gorges Area, the base of the Hamajing Member consists of wavy beds of massive dolomite. The base of the Shibantan Member is characterized by thinly bedded limestone followed by a succession of dark, macrocrystalline limestone beds, a few intercalated chert layers and chert nodules. The top of the Shibantan Member is rich in chert nodules and possibly grades into the Baimatuo Member with low amplitude wavy bedding of the carbonates.

The depositional environment of the Dengying Formation is interpreted in terms of a prograding platform. Oolitic textures and oncolites in the dolomitic Hamajing Member are characteristic of a shallow, high-energy environment following black shale deposition at the top of the Doushantuo Formation, indicating a sea-level drop from the Doushantuo to the Dengying Formation (Zhu *et al.*, 2007, 2013). Towards the south-east, the carbonate successions become gradually thinner, ultimately changing into the slope and basinal facies of the corresponding Liuchapo Formation, which is mainly composed of black silicified shales that in places reach into the early Cambrian (e.g. Wang *et al.*, 1998; Chang *et al.*, 2009).

Studied sections

At the Huanglian section, Guizhou Province, stratigraphic control is rather poor, but an equivalent level there to the Liuchapo Formation was sampled, consisting of black silicified shale below a black shale succession. The nearby Longbizui section, Hunan Province, on the other hand, offers an excellent transitional succession from cherty shales and bedded cherts of the predominantly Late Ediacaran Liuchapo Formation, to the black shales of the Early Cambrian Niutitang Formation.

Early Cambrian formations

The global standard stratotype-section and point (GSSP) for the base of the Cambrian System is the first appearance datum (FAD) of the trace fossil *Trichophycus (Treptichnus) pedum* (Brasier *et al.*, 1994; Landing, 1994; Babcock & Peng, 2007). However, due to a lack of convincing evidence for the occurrence of this trace fossil in Cambrian sediments in South China and absolute age constraints (Compston *et al.*, 1992, 2008; Yang *et al.*, 1996; Jenkins *et al.*, 2002; Jiang *et al.*, 2009; Och *et al.*, 2013), correlation of the Precambrian–Cambrian boundary focuses instead on the biostratigraphy of small shelly fossils (Steiner *et al.*, 2007), as well as C-isotope stratigraphy (for example, at the Meishucun section sampled for this study; Cowie, 1985; Luo *et al.*, 1992; Shields *et al.*, 1999; Zhu *et al.*, 2003). Because of the strongly varying abundance of small shelly fossils on the Yangtze Platform, phosphorite horizons occurring in the lowermost Cambrian have also been taken into account in the present study, where the Precambrian–Cambrian boundary was not obvious stratigraphically.

The Niutitang Formation

The Niutitang Formation, which is locally strongly condensed, comprises mainly black shales, siltstones, intercalated chert, organic-rich carbonates and phosphate nodules. It predominantly crops out within the transitional belt at the platform margin and, often uncomformably, overlies the Dengying/Liuchapo formations. Phosphorite beds at the base of the Niutitang Formation and organic-rich black shales above can be used as marker horizons across the slope and basin of the Yangtze Platform; these have predominantly been studied because of an extreme enrichment of Ni and other metal sulphides, in particular Mo with concentrations up to several per cent (e.g. Och *et al.*, 2013, and references therein).

Studied sections

The base of the Niutitang Formation has been sampled at the basinal Huanglian and Longbizui sections, and mainly consists of an uninterrupted black shale succession. In the more extensively sampled Longbizui section, two distinct layers of pyrite and carbonate concretions have been found above the Liuchapo–Niutitang boundary.

The Yanjiahe and Shuijingtuo formations

The Yanjiahe Formation, which covers the Precambrian–Cambrian transition south of the Huangling anticline in the Three Gorges Area, overlies pale, massive dolomites of the Dengying Formation (Baimatuo Member) above a sharp, wavy contact. The Yanjiahe Formation is *ca* 35 m thick and consists of dolomitic muddy limestone, calcareous black shale and some sandstone and chert (Ishikawa *et al.*, 2008). The overlying Shuijingtuo Formation is *ca* 100 m thick and mainly consists of black shale with prominent carbonate concretions (Ishikawa *et al.*, 2008). Mainly based on carbon isotope stratigraphy, it is likely that the upper part of the Yanjiahe Formation is equivalent to the Dahai Member of the Early Cambrian Zhujiaqing Formation (Li *et al.*, 2013; Cremonese *et al.*, 2014), while the presence of sponge spicules and trilobite fragments suggests that the overlying Shuijingtuo Formation could be considerably younger, possibly even Cambrian Stage 3.

Studied sections

The sampling of the Yanjiahe and Shuijingtuo formations was conducted at the Jijiapo and Jiuqunao section where the base of the Yanjiahe Formation is characterized by grey carbonate beds with thin chert intercalations. Abundant phosphatic cherts were recognized in the middle part of the formation, whereas massive dolomite beds, followed by organic-rich black dolomite interbedded with siltstone, including regularly shaped silicified carbonate nodules, occur in the upper part below the boundary to the Shuijingtuo Formation The boundary zone is characterized by a thin (*ca* 10 cm) phosphorite bed, followed by a conglomeratic layer with rip-up clasts and framboidal pyrite. The basal Shuijingtuo Formation consists of black shales with abundant, metre-sized dolomite concretions and some intercalated grey massive dolomite beds.

MATERIALS AND METHODS

One hundred forty-three well-preserved predominantly black shale samples and some more or less organic-rich carbonate samples were collected at seven localities during two field seasons (2008 and 2009) on the Yangtze Platform, from the Doushantuo Formation Member II to the early Cambrian Shuijingtuo Formation. Sampling steps vary considerably between highly resolved segments of decimetre-scale to broad steps of over 10 m. All of the present samples were converted into powders using a tungsten carbide mill.

Geochemical analyses included X-ray fluorescence carried out on a Philips PW2400 spectrometer (PANalytical, Almelo, The Netherlands) for major and trace elements on 54 samples collected during the first field season (Maoshi, Huanglian and Longbizui). The 89 samples collected during the second field season in the Three Gorges Area (Jiulongwan, Jiuqunao, Yangjiahe and Jijiapo) were dissolved after ashing at 550°C before analysis for bulk elemental composition using ICP-MS and Fe speciation. In detail, 5 ml of nitric acid was added to the ashed powder, before adding 2 ml of hydrofluoric acid and a few drops of $HClO_4$. The sample was then dissolved on a hot plate. After evaporation, 2·5 ml of boric acid (50 g l^{-1}) acid was added and evaporated to dryness on a hot plate to dissolve any aluminium hexafluorates. The samples were then taken up in 5 ml of hot 50% HCl. Iron speciation analysis was carried out on all samples according to the method outlined by Poulton & Canfield (2005). The present authors measured the concentrations of four different highly reactive iron phases (Fe_{HR}): pyrite iron (Fe_{Py}), carbonate-associated iron (Fe_{carb}), ferric oxides (Fe_{ox}) and magnetite iron (Fe_{mag}), and total iron content (Fe_T); Fe_{Py} was determined via the chromous chloride technique of Canfield *et al.* (1986), while AVS (FeS) was only detected in trace amounts. The sequential extraction procedure of Poulton & Canfield (2005) was used to determine the other highly reactive iron phases, specifically Fe_{carb}, Fe_{ox} and Fe_{mag}. To determine Fe_T, *ca* 100 mg sample powder was dissolved using the above-mentioned method for total dissolution and then diluted 50 times. All solutions were analysed for their respective iron contents using an atomic absorption spectrometer (AAS), with a relative standard deviation (RSD) of <5% for all stages. The same sample solutions were then evaporated to dryness and redissolved in

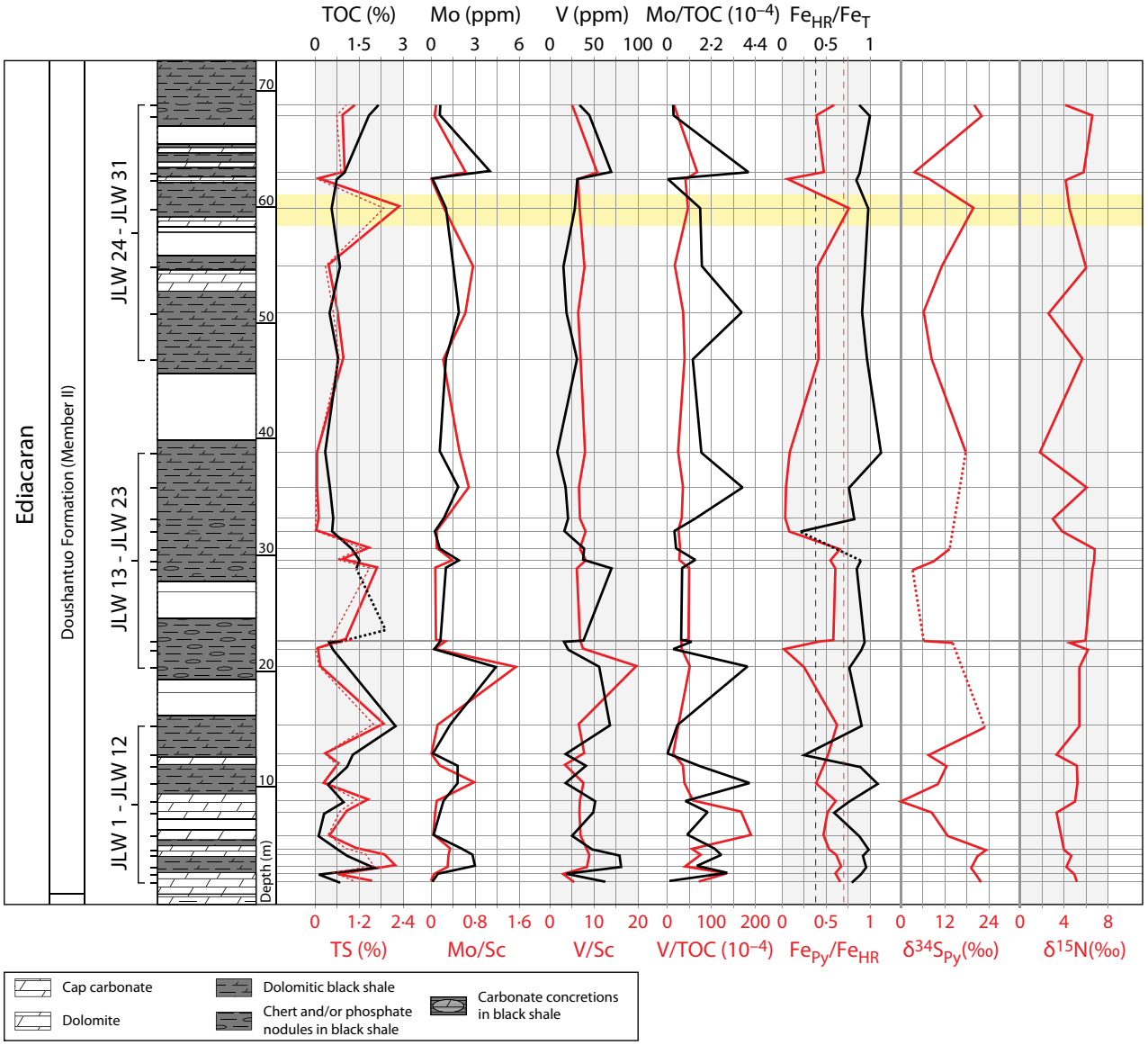

Fig. 3. Stratigraphy and geochemical profiles across the Doushantuo Member II at the Jiulongwan section, Hubei Province. Note that, due to extensive vegetation, considerable gaps along the stratigraphy had to be taken into account. The analysed samples are indicated on the left. The yellow shaded sections show deposition under possibly euxinic conditions indicated by Fe_{Py}/Fe_{HR} ratios above 0·7 (red dashed line). Anoxic conditions are indicated by Fe_{HR}/Fe_T ratios above 0·38 (black dashed line): TOC, total organic carbon; TS, total sulphur; Fe_T, total iron; Fe_{HR}, highly reactive iron; Fe_{Py}, pyrite iron.

nitric acid in order to measure the trace-metal contents. The final solution, containing 0·15 ml HNO_3, 0·1 ml 500 ppb Re for instrument calibration and 3·75 ml H_2O, was analysed at the State Key Laboratory for Mineral Deposits Research, Nanjing University, using a Finnigan Element II inductively coupled plasma mass spectrometer (ICP-MS; Thermo Fisher Scientific Inc, Waltham, MA, USA). The precisions were generally better than 5% for the analysed elements based on long-term uncertainty of the laboratory measurement on a standard carbonate sample.

Samples which yielded enough Ag_2S residue (>0·03 g) after the sulphide extraction procedure were analysed for sulphide isotopes using a Finnigan MAT DeltaPlus plumbed to a Carlo Erba elemental analyser through a Conflo II interface (CE Elantech Inc, Lakewood, NJ, USA). All analytical work for sulphur isotopes was carried out at the Institute for Geology and

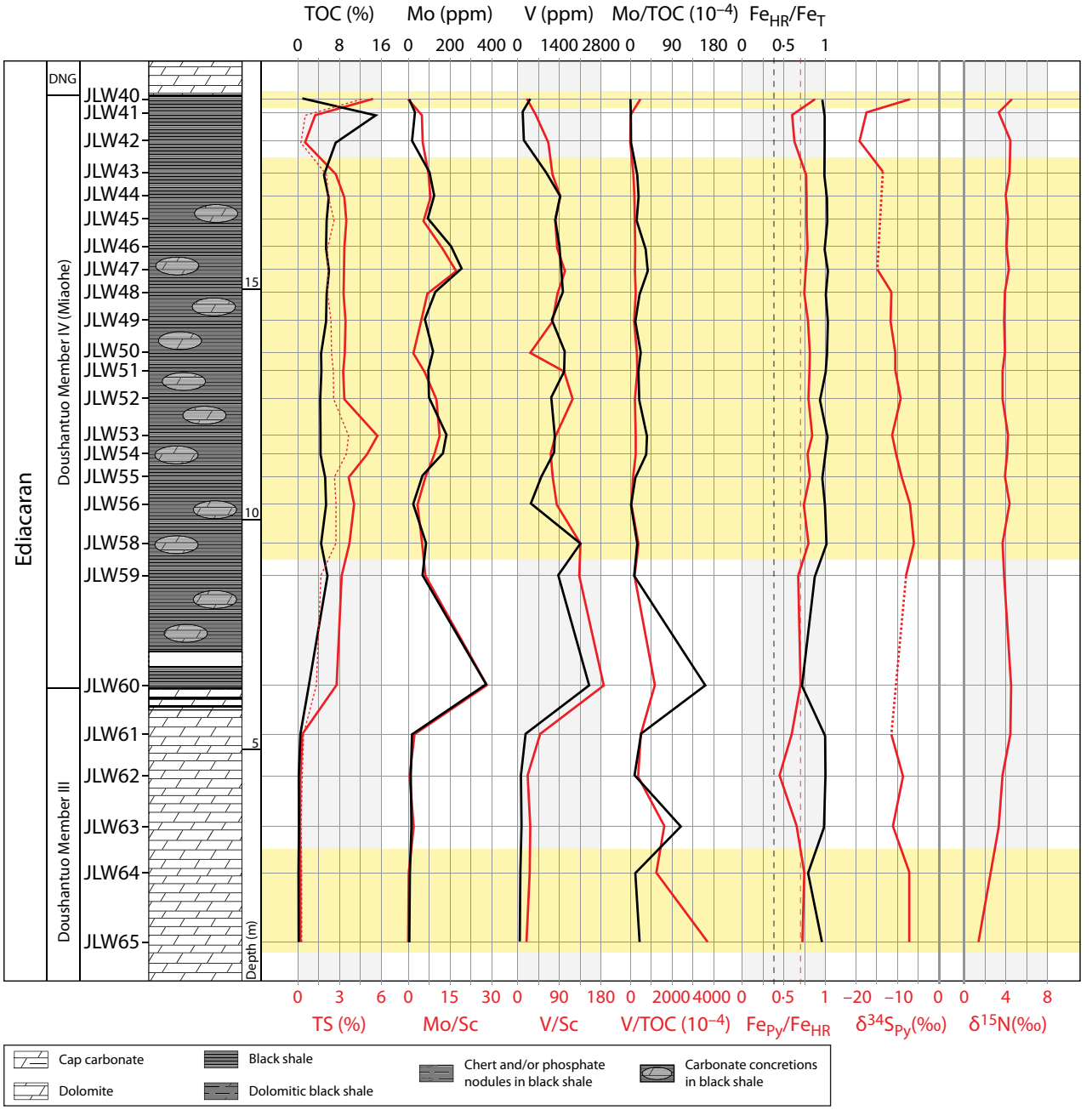

Fig. 4. The upper part of member III and the complete member IV (Miaohe) of the Doushantuo Formation at Jiulongwan. See Fig. 3 for abbreviations and formatting. DNG = Dengying.

Paleontology, Westfälische Wilhelms-Universität Münster, Germany. Nitrogen isotopic analyses have previously been published in Cremonese *et al.* (2014) and the methods are described therein.

The evaluation of TOC, total carbon (TC) and total sulphur (TS) was carried out using a Leco C/S analyser (Leco Corporation, St Joseph, MI, USA) at the Wolfson Laboratory, University College London. The TC and TS were measured directly after weighing between 100 mg and 300 mg of sample powder. The TOC content was determined after dissolving each sample with 10% HCl at room temperature until no effervescence was observed, followed by filtering and rinsing with H_2O prior to introducing the dried remains into the C/S analyser.

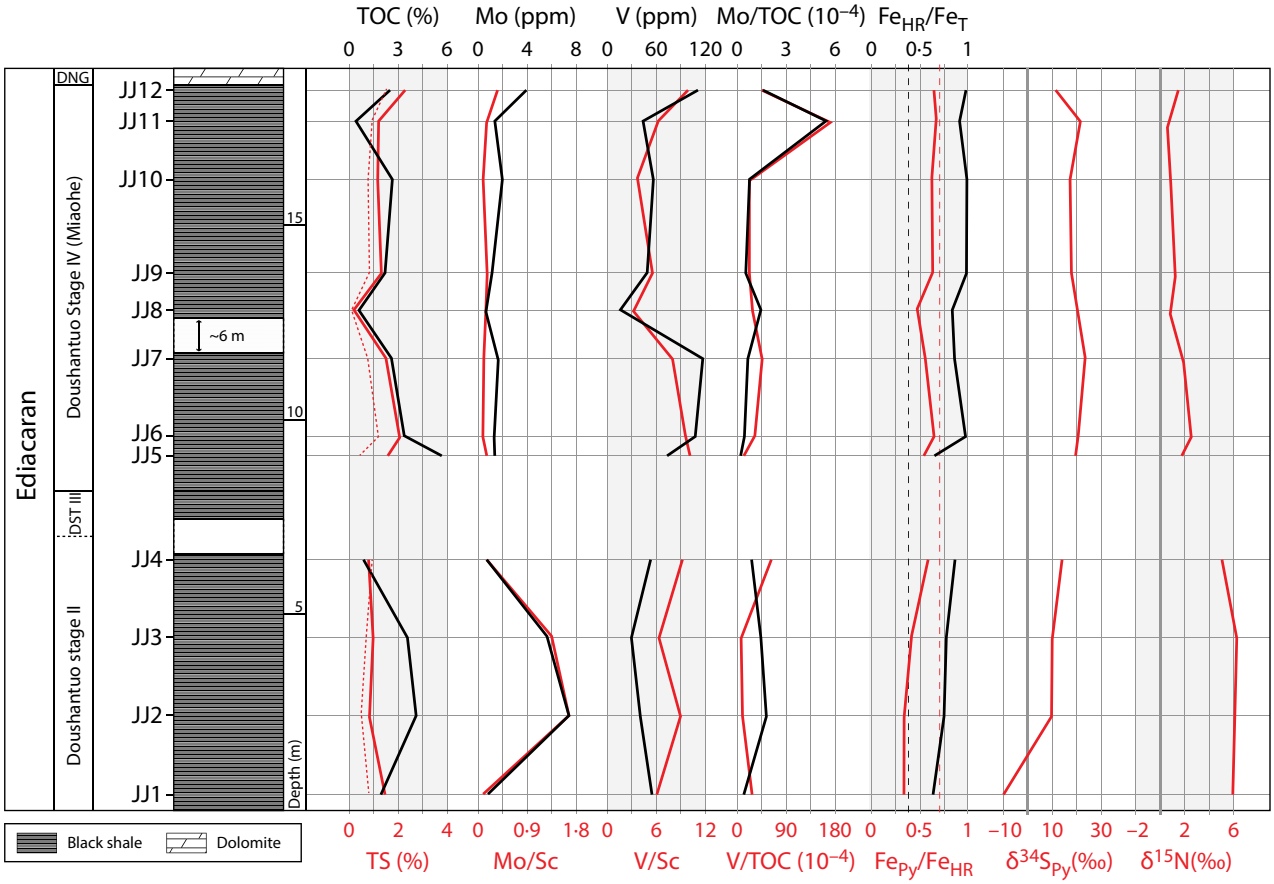

Fig. 5. Stratigraphy and geochemical profiles for the black shales of the Doushantuo members II and IV at the Jiuqunao section. The distance between the members DST II and DST IV is unknown. Note that Fe_{Py}/Fe_{HR} ratios reach high values within DST IV but are not high enough to be identified as a euxinic depositional environment. See Fig. 3 for abbreviations and formatting. DNG = Dengying.

RESULTS

The Doushantuo Formation

The extensive Jiulongwan sections (JLW) in the Three Gorges Area, Hubei Province, span from Doushantuo Member II (DST II) to Doushantuo Member IV (DST IV). For these sections, Mo and V concentrations mostly remain well below average shale values, until the onset of DST IV (Figs 3 and 4). In this late Ediacaran black shale succession, Mo concentrations reach *ca* 370 ppm, with concomitant V concentrations of over 2400 ppm found just at the onset of black shale deposition in DST IV. Molybdenum correlates only moderately with V, with a more significant correlation within DST IV (R^2 = 0·53) than DST II (R^2 = 0·25). Total organic carbon shows no significant correlation with Mo, but is weakly correlated with V (R^2 = 0·34) within the lower DST II, where TOC contents are generally below 1% but with a few peaks of up to 2·4%. Within DST IV, no significant correlation is found between trace-metals and TOC contents, where TOC rises smoothly after the DST III/DST IV boundary, stabilizes between 4 wt% and 6 wt %, and reaches a maximum concentration of 14·9% towards the top. Total sulphur and pyrite sulphur correlate well throughout the section, but in particular within DST II, where less non-pyrite sulphur is found within DST IV. The Mo/TOC ratios within DST II are highly variable, ranging up to 4×10^{-4}. The Mo/TOC ratio reaches a maximum of 180×10^{-4} at the bottom of DST IV and rapidly declines to oscillate between 0 and slightly above 40×10^{-4}. Iron speciation analysis suggests deposition under anoxic conditions, with DST II sediments indicating a ferruginous water column (Fe_{HR}/Fe_T > 0·38; Fe_{py}/Fe_{HR} < 0·7 to 0·8) and the overlying

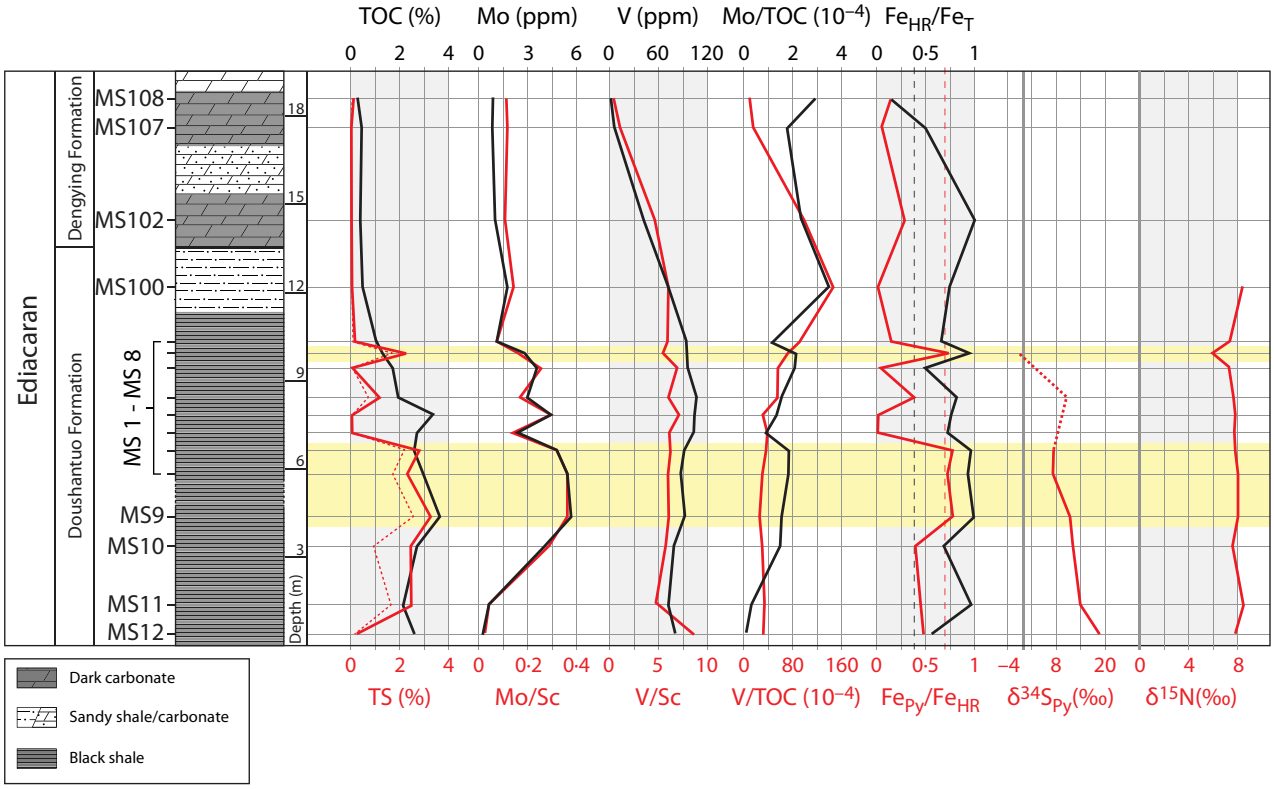

Fig. 6. The stratigraphy and geochemical profiles at the Maoshi section, Guizhou Province. See Fig. 3 for abbreviations and formatting.

DST IV indicating at least intermittently euxinic conditions $Fe_{HR}/Fe_T > 0{\cdot}38$; $Fe_{py}/Fe_{HR} > 0{\cdot}7$ to 0·8).

The pyrite $\delta^{34}S$ profile is very variable but initially positive with values between 0‰ and 23‰ within DST II (Fig. 3). Further up in the Doushantuo Formation (Fig. 4), a decline occurs from *ca* −7‰ within the carbonates of DST III, to −19‰ within the upper part of the Miaohe black shale (DST IV), which is followed by a steep increase back to −7‰ below the Doushantuo/Dengying boundary. Within DST II, $\delta^{15}N$ values are also positive and vary between 1·9% and 6·7‰ without any particular trend (Fig. 3). In the upper part of DST III the $\delta^{15}N$ profile exhibits an increase from 1·3 to 4·3‰ towards the Miaohe Member, at which value they remain approximately except for a single, minor excursion down to 3·2‰ at the top (Fig. 4).

Throughout the Doushantuo Formation at the Jiuqunao section (JJ), Hubei Province, very low redox-sensitive trace-metal concentrations close to average shale were measured (Fig. 5). Anoxic conditions can, however, be inferred from iron speciation analysis throughout the section but, although relatively high Fe_{Py}/Fe_{HR} ratios of between 0·6 and 0·7 are common within the black shale of DST IV, there is no convincing evidence for euxinic water column conditions. The $\delta^{34}S$ values for pyrite show a sharp increase from −10 to +10‰ within DST II and remain at this approximate level. In the Miaohe Member, $\delta^{34}S$ values are *ca* +15‰ and exhibit a decrease down to +10‰ 1 m below the Doushantuo/Dengying boundary. The $\delta^{15}N$ profile basically shows a decrease from values between 5‰ and 6‰ within DST II, to values that decrease from 2·5 to 0·6‰ in the Miaohe Member.

The Maoshi section (MS), in Guizhou Province spans the boundary between the late Ediacaran Doushantuo and Dengying formations, and exhibits average shale Mo and V concentrations of *ca* 3 ppm and 100 ppm, respectively (McLennan, 2001; Fig. 6). The TOC contents are high in the upper Doushantuo Formation (1 to 3·4%) and fall below 1% in the overlying Dengying Formation, with only a weak correspondence between peaks in TOC and TS. The correlation between the trace-metals and TOC and TS is weak but the highest Mo and V con-

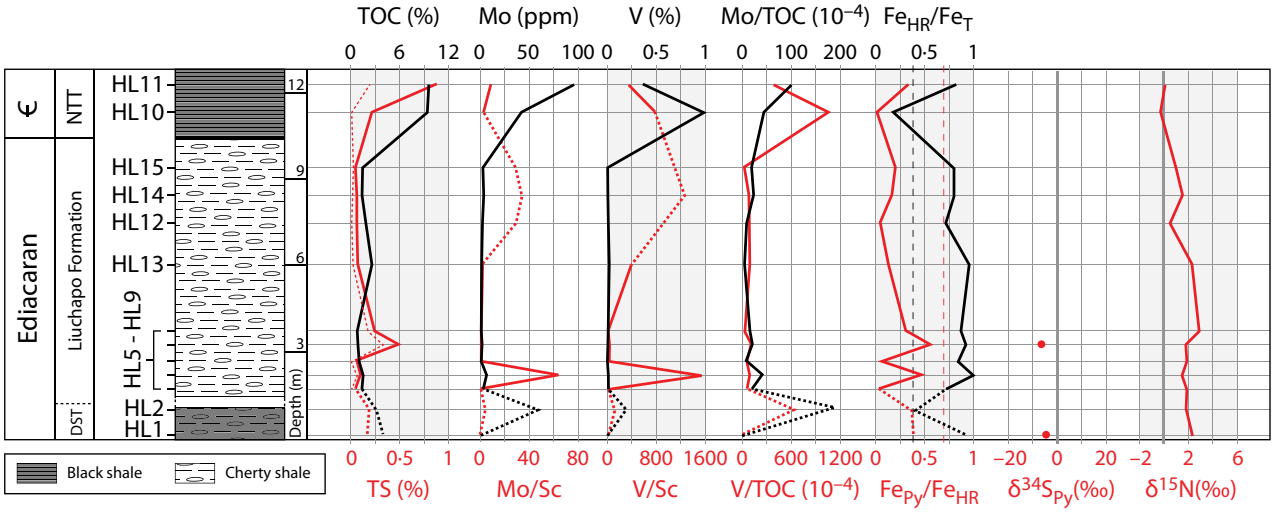

Fig. 7. The Huanglian section, Guizhou Province, with the stratigraphy across the Precambrian–Cambrian boundary and the relevant geochemical profiles. Note that two samples are from the Doushantuo Formation which underlies the Liuchapo Formation but, as the stratigraphic control is poor in this region, the scale is unknown. See Fig. 3 for abbreviations and formatting. ∈ = Cambrian; NTT = Niutitang Formation.

centrations are mostly concomitant with the highest TOC and TS values. There is a very strong correlation between TS and pyrite S, but with a significant excess of non-pyrite S. The Mo/TOC ratios show a slightly increasing trend towards the top of the Doushantuo Formation but remain very low, with a maximum of $3{\cdot}4 \times 10^{-4}$. Iron speciation indicates anoxic-ferruginous conditions with possibly intermittent euxinia in the upper Doushantuo Formation, suggested by Fe_{Py}/Fe_{HR} ratios of up to 0·77. The $\delta^{34}S$ values for pyrite recovered from the black shale of the upper Doushantuo Formation exhibit a decreasing trend from 18·5 to −1·5‰, while the $\delta^{15}N$ profile for the same samples is quite constant with high values of *ca* +8‰.

The Late Ediacaran (Dengying/Liuchapo formations) and Early Cambrian formations

The Huanglian section, Guizhou Province, which covers the Precambrian–Cambrian transition from the Liuchapo (equivalent) Formation to the Niutitang Formation, exhibits significant variability in trace-metal concentrations (Fig. 7). Maxima of 96 ppm for Mo and 9860 ppm for V at the base of the Niutitang Formation coincide with very high TOC contents of up to 9·6%, leading to a moderate correlation between Mo, V and TOC. Sulphur contents are relatively low and a moderate correlation between TS and pyrite S prevails, with substantial non-pyrite S at the base of the Niutitang Formation Nevertheless, Mo concentrations correlate relatively well with TS ($R^2 = 0{\cdot}67$), indicating that Mo is efficiently scavenged into sulphidic sediment even when pyrite formation is minor. A relatively high Mo/TOC ratio of 19×10^{-4} is found within sediments of the upper Doushantuo Formation, while low values prevail within the Liuchapo Formation, increasing again at the base of the Niutitang Formation, where a maximum Mo/TOC ratio of 10×10^{-4} is found. An anoxic-ferruginous depositional environment is clearly indicated by Fe speciation analysis, with Fe_{Py}/Fe_{HR} ratios that vary considerably but remain low at between 0·01 and 0·56. Due to a lack of pyrite, only two samples could be analysed for $\delta^{34}S$, yielding −4·3‰ and −6·3‰. The $\delta^{15}N$ values are low, but positive, with values no higher than 2·4‰ in the Liuchapo Formation, decreasing to *ca* 0‰ in the Lower Cambrian Niutitang Formation.

Within the predominantly cherty shales and chert beds of the Liuchapo Formation at the Longbizui section (LBZ), a thin black shale interval is found where TOC and TS concentrations both reach over 3·1% within a thin horizon, while Mo and U remain depleted and V is only slightly enriched, with concentrations of up to 340 ppm (Fig. 8). The Fe_{Py}/Fe_{HR} ratios exceed 0·7 within an interval of 15 cm just below and within this organic-rich horizon, below which $\delta^{34}S_{pyrite}$ values range widely

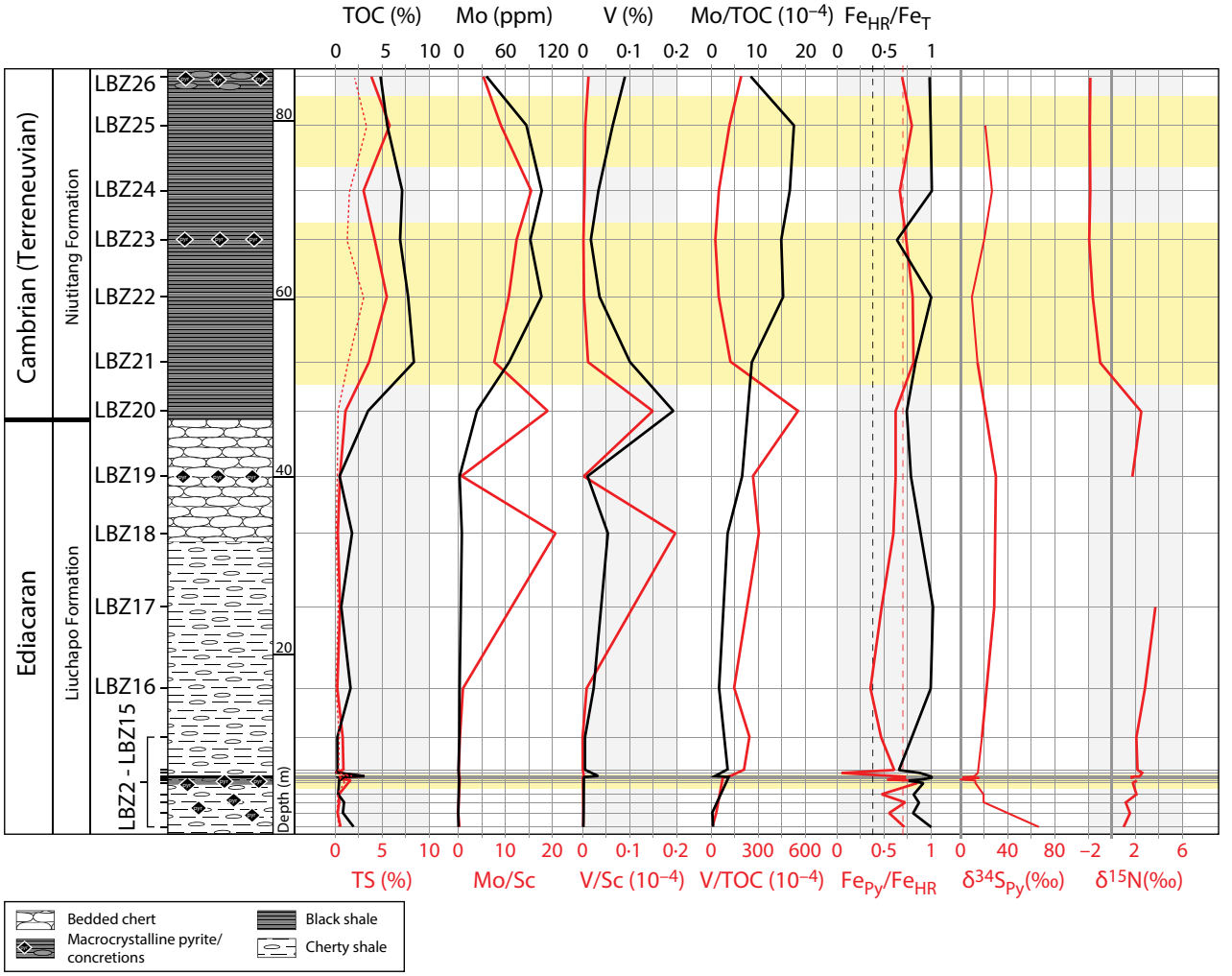

Fig. 8. The geochemical profile at the Longbizui section, Guizhou Province. See Fig. 3 for abbreviations and formatting.

between +66‰ and a minimum of −0·38‰. The overlying Liuchapo Formation is characterized by TOC and TS contents below 1% and relatively low trace-metal concentrations, with V up to 1937 ppm and Mo up to 107 ppm, broadly tracking TOC and TS contents. The TS contents correlate well with pyrite S, although variable amounts of non-pyrite S (averaging 50% of TS) are observed. The Mo/TOC ratios are low prior to the Niutitang Formation, where they reach values of between $7{\cdot}0 \times 10^{-4}$ and $15{\cdot}8 \times 10^{-4}$. On the other hand, V/TOC ratios show a maximum of 553×10^{-4} just below the Niutitang black shales, and decrease to low values of between 26×10^{-4} and 190×10^{-4} further up. The Fe_{HR}/Fe_T ratios indicate anoxic conditions throughout the section, and Fe_{Py}/Fe_{HR} ratios between 0·7 and 0·8 suggest possibly sulphidic conditions during extended intervals within the Niutitang black shale. Sulphide isotope values remain positive throughout the remaining section, $\delta^{34}S$ being enriched by between 9·3‰ and 29·6‰. The $\delta^{15}N$ profile exhibits higher values of between 1‰ and 3·7‰ within the Liuchapo Formation, which decrease sharply to negative values of *ca* −2‰ at the Liuchapo/Niutitang Formation boundary.

The Jijiapo section (YS), Hubei Province, includes samples from the Lower Cambrian formations which are strongly depleted in Mo within the organic-poor Yanjiahe samples, but show enrichment within the overlying Shuijingtuo Formation, where Mo reaches concentrations of up to 37 ppm and Mo/TOC ratios up to 32×10^{-4} (Fig. 9). Good correlation is observed between TS and Mo contents ($R^2 = 0{\cdot}92$),

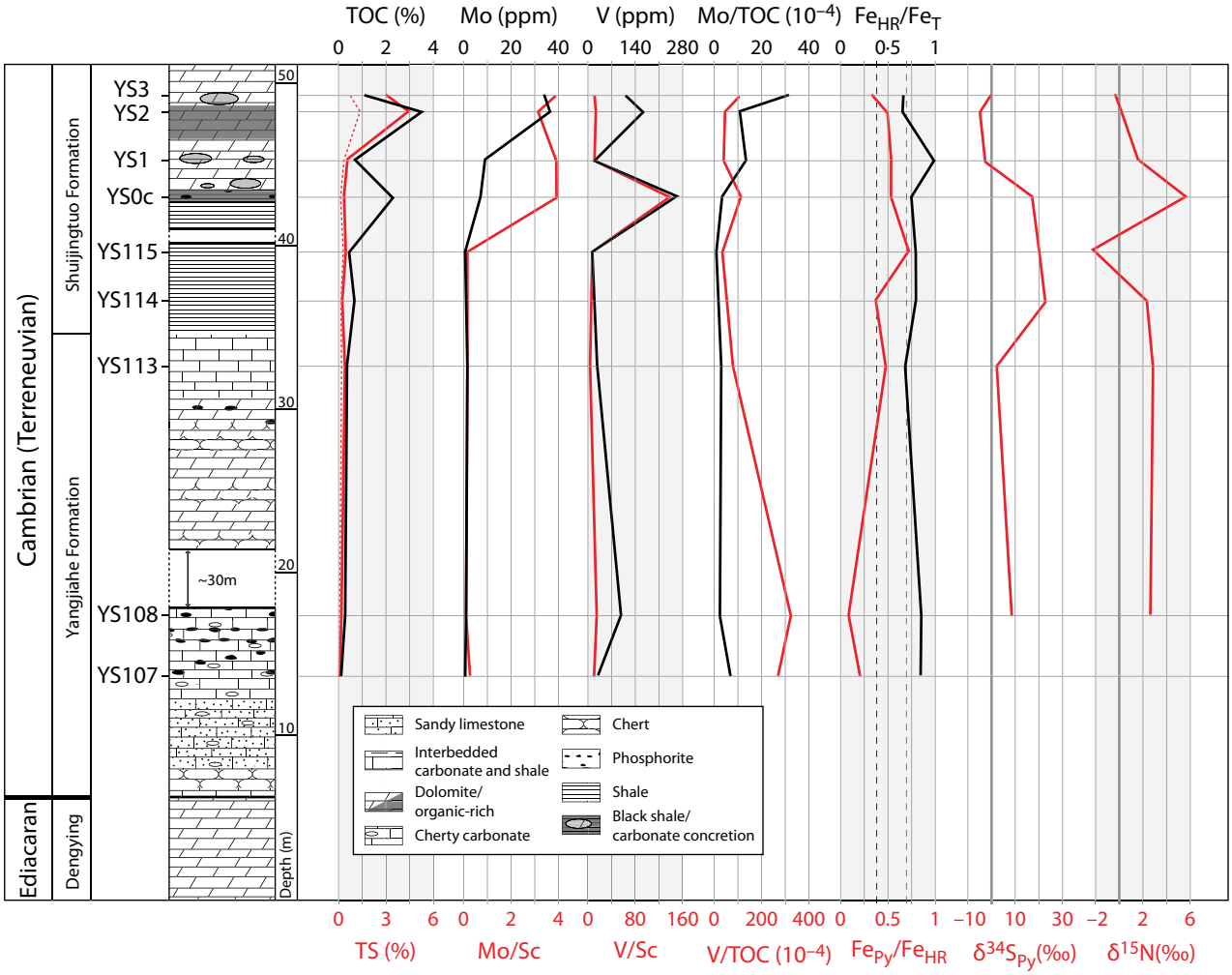

Fig. 9. Stratigraphy and geochemical profiles at the Jijiapo section, Hubei Province. See Fig. 3 for abbreviations and formatting.

whereas V concentrations are significantly better correlated with TOC (R^2 = 0·61). While TS correlates with pyrite sulphur, a great excess of non-pyrite sulphur was observed. Iron speciation analysis supports anoxic-ferruginous conditions without evidence for sustained euxinia. The $\delta^{34}S$ values within samples from the organic-poor Yangjiahe Formation are all positive, with an increase from values of *ca* 5‰ to over 23‰ beneath the overlying Shuijingtuo Formation, followed by a subsequent decrease down to −5‰. The $\delta^{15}N$ profile shows constant values of slightly below 1‰ within the Yanjiahe Formation except at the top, where values of between −2·3‰ and +5·6‰ occur within the lowermost Shuijingtuo Formation.

At the Jiuqunao section (JJL), redox-sensitive trace-metal concentrations are significantly enriched in the lower Cambrian black shales of the Shuijingtuo and Yanjiahe formations (Fig. 10). At the onset of the black shale succession of the Shuijingtuo Formation, Mo peaks at 213 ppm with a concomitant peak in V concentration of 910 ppm, before concentrations decrease to relatively constant values of *ca* 40 ppm and 150 ppm, respectively, with an overall good correlation between Mo and V (R^2 = 0·95). The Mo/TOC ratios track the Mo concentration profile, attaining a maximum of 36×10^{-4}. Total organic carbon, TS and pyrite sulphur also correlate well within the Early Cambrian formations, where a significant amount of non-pyrite sulphur is present. In the Shuijingtuo Formation, frequent euxinic conditions are plausible with Fe_{Py}/Fe_{HR} ratios between 0·7 and 0·8. Interestingly, the maximum peaks in Mo and V

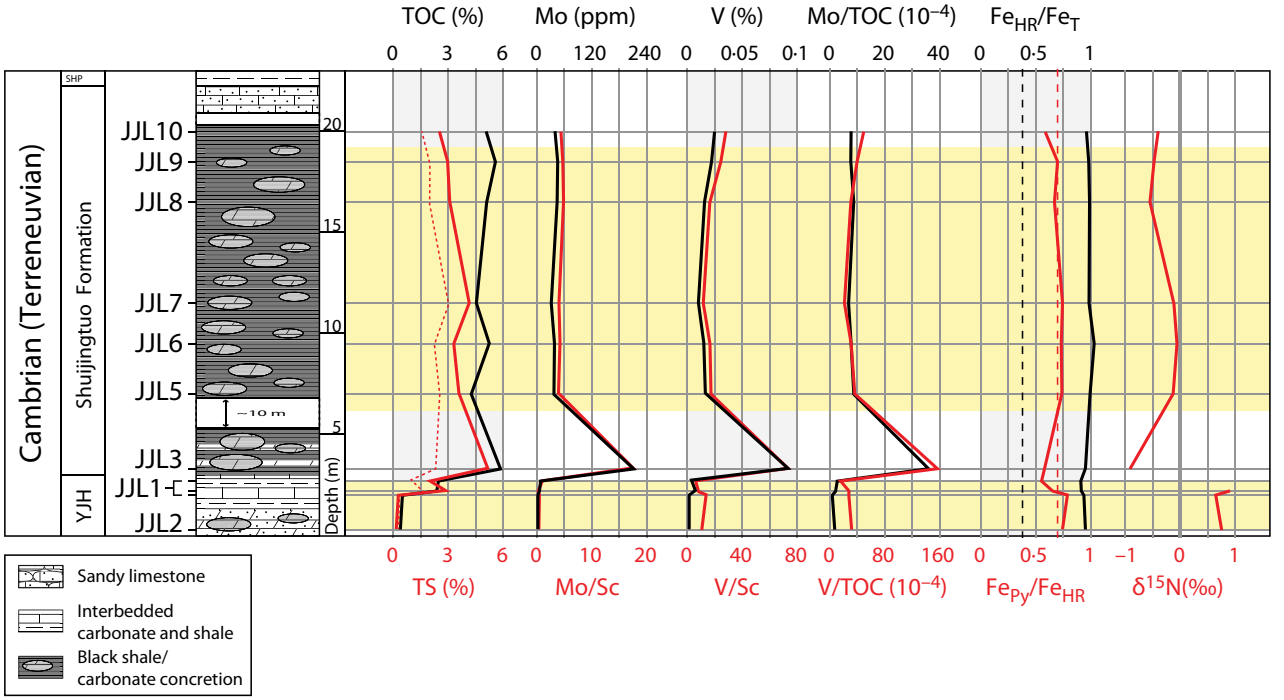

Fig. 10. The early Cambrian Shuijingtuo Formation at the Jiuqunao section, Hubei Province. See Fig. 3 for abbreviations and formatting. YJH = Yanjiahe Formation; SHP = Shipai Formation.

contents occur at the stratigraphic level where Fe_{Py}/Fe_{HR} ratios are particularly low. In the Shuijingtuo Formation, the one carbonate sample (JJL1) analysed for its $\delta^{34}S$ signature within the lower Shuijingtuo Formation has a value of 18·6‰. Similarly, only a few $\delta^{15}N$ values were measured, but they show a clear decrease from *ca* 0·8‰ within the carbonate samples at the bottom, to *ca* −0·5‰ in the TOC-rich black shale further up, before a slight increase (but remaining negative) for the rest of the section.

DISCUSSION

Figures 11 and 12 summarize the most important geochemical indicators considered in the present study. Figure 11 focuses on the Ediacaran and Cambrian strata found in the Three Gorges Area and also includes Mo/TOC and V/TOC ratios of the Baiguoyuan section north of the Huangliang granite (reported by Wallis, 2006). Figure 12 shows the data for the Precambrian/Cambrian transition at Huanglian and Longbizui which were deposited in a basinal setting. The Xiaotan section, at the boundary between the Yunnan and Sichuan provinces (Fig. 2), contains an unusually expanded Early Cambrian succession to the north-west of the Yangtze Platform. The trace-metal concentrations and iron speciation analyses have previously been reported by Och *et al.* (2013) and the nitrogen isotope signature by Cremonese *et al.* (2013). These results are summarized here and include a previously unpublished $\delta^{34}S$ profile (Fig. 13). The most significant geochemical feature is the relatively low Fe_{HR}/Fe_T ratio within the Yuanshan Formation, down to 0·2 at the top, which indicates that the sediments were potentially deposited beneath an oxic water column (see Supporting Information; Poulton & Canfield, 2011).

In the last few years, research on biogeochemical cycling on the Yangtze Platform during the Late Ediacaran has intensified. Li *et al.* (2010), Sahoo *et al.* (2012) and, more recently, Kikumoto *et al.* (2014), have contributed greatly to the growing understanding of the processes that prevailed during the Precambrian–Cambrian transition and presented datasets that complement the findings of the present study (Fig. 14). The study by Li *et al.* (2010) introduced the concept of a sulphidic wedge during deposition of the Miaohe Member (DST IV) to explain Mo enrichment at Jiulongwan, while little Mo

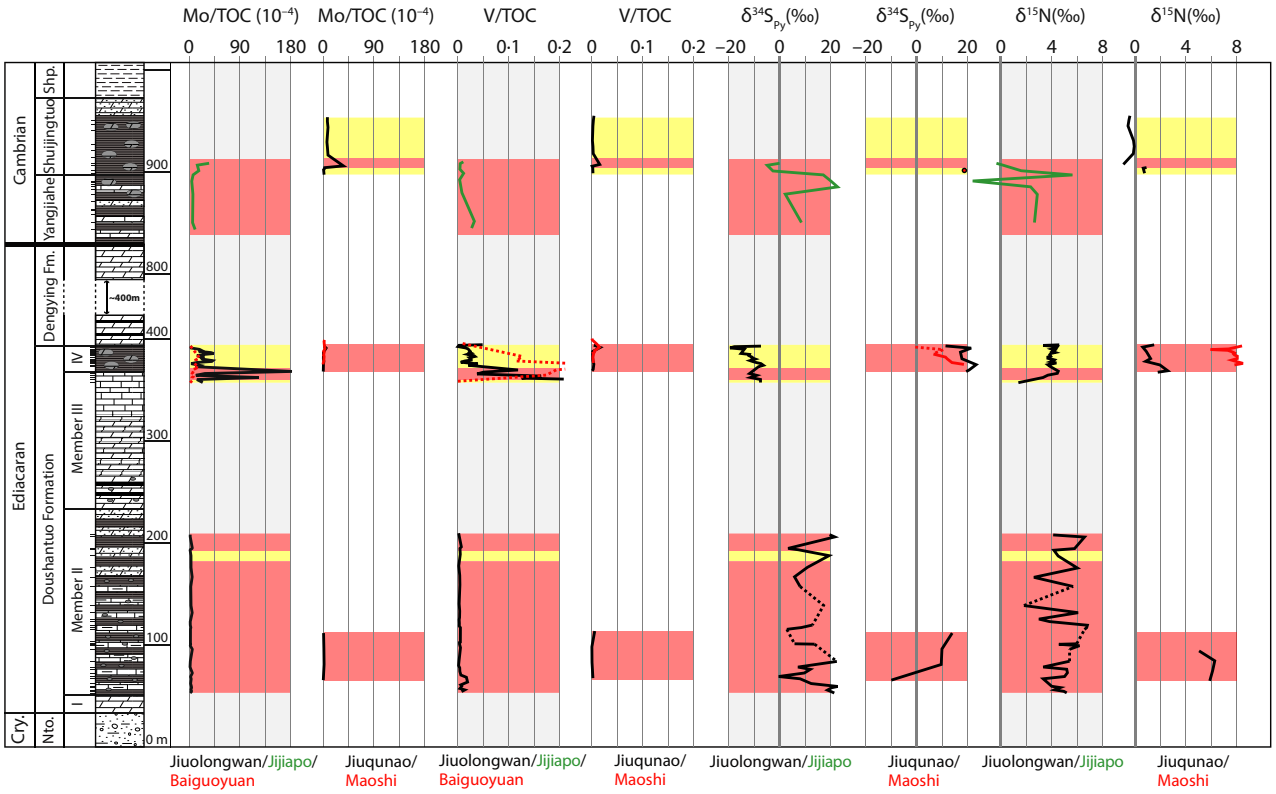

Fig. 11. Schematic summary plot for all sections sampled in the Three Gorges Area including the Maoshi section, Guizhou Province, which is situated *ca* 530 km to the south-west (see Fig. 2). The reddish shaded intervals indicate anoxic-ferruginous conditions and the yellow shaded intervals suggest a euxinic depositional environment. Note the very low Mo and V enrichment relative to TOC and the almost exclusively positive $\delta^{34}S$ values within the DST II. While this phenomenon persists until the Cambrian within the Jiuqunao and Maoshi sections, a massive trace-metal enrichment is observed in the Jiulongwan and Baiguoyuan sections within the Maoshi Member alongside negative $\delta^{34}S$ values at Jiulongwan. Cry = Cryogenian Period; Nto = Nantuo Formation; Shp = Shipai Formation.

sequestration occurred at Zhongling *ca* 100 km in the south. These authors used a simplified platform-basin model and concept that has recently been disputed by Cui *et al.* (2015) on the basis of a revised chemostratigraphic framework. On the other hand, Sahoo *et al.* (2012) presented a substantial Mo enrichment further south and earlier in time during the deposition of DST II. In all sections high Mo/TOC ratios coincide with lower $\delta^{34}S$ values, indicating an association between euxinic conditions and the spread of sulphate (and Mo) enriched waters.

The present study aims to shed light on a crucial time in Earth history, the Neoproterozoic Oxygenation Event (NOE), when changing redox conditions in the ocean were succeeded by an unprecedented rise in the diversity and architectural complexity of organisms. Within this context and using a multiproxy elemental and isotopic approach, the palaeobathymetric situation and the degree of restriction of the regional and local marine environments on the Yangtze Platform during this transition can better constrain the framework for the NOE.

The Nantuo Formation, deposited during the end-Cryogenian 'Marinoan' Glaciation, represents the last stage of the rifting history of the Yangtze Platform, which left a sea floor with abundant horst and graben structures, onto which sediments of the Doushantuo Formation have been draped (e.g. Vernhet, 2007; Zhu *et al.*, 2013). In addition, the Huangling granite intrusion and its subsequent erosion during multiple phases of glaciations are likely to have had a major impact on the bathymetry of the Three Gorges Area, in particular. A mosaic of different depositional environments can therefore be imagined, which has been confirmed by studies demonstrating significant lateral facies varia-

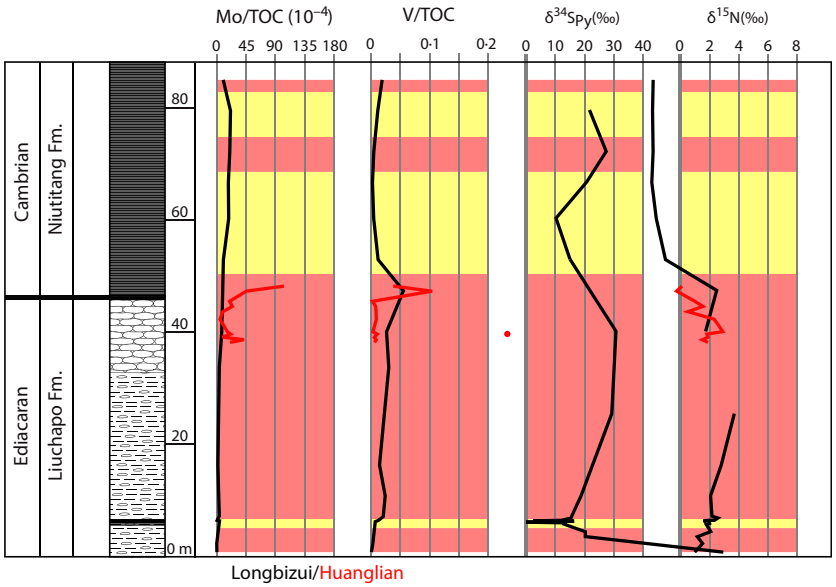

Fig. 12. Mo and V concentrations normalized to TOC, pyrite sulphur and nitrogen isotopes for the basinal sections at Longbizui and Huanglian. Note that the Mo/TOC and V/TOC increase at the base of the Cambrian and the concurrent decrease of $\delta^{34}S$ and $\delta^{15}N$ values.

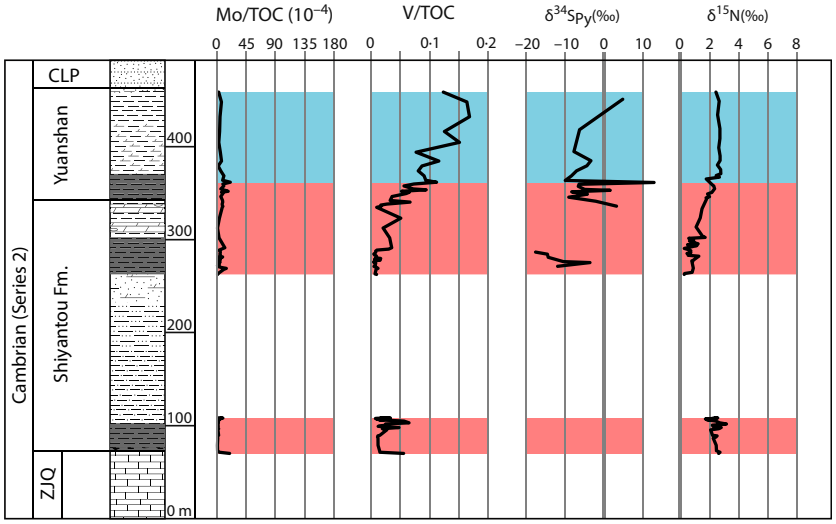

Fig. 13. Summary of geochemical results from the Early Cambrian Xiaotan section (Cremonese *et al.*, 2013; Och *et al.*, 2013). ZJQ = Zhujiaqing Formation; CLP = Canglangpu Formation.

tions, notably around the Three Gorges Area (e.g. Vernhet & Reijmer, 2010; Jiang *et al.*, 2011; Zhu *et al.*, 2013). The stratigraphic and palaeoenvironmental ambiguity, however, has contributed to a wealth of different ideas on the depositional environment of the Doushantuo Formation, i.e. whether it was deposited in a non-marine basin (Bristow *et al.*, 2009), an intra-shelf basin (Vernhet & Reijmer, 2010) or a shelf lagoon (Jiang *et al.*, 2011). The sections below begin by evaluating environmental conditions during deposition of the Doushantuo Formation, and then expand this palaeoenvironmental analysis to track environmental conditions into the Early Cambrian.

The Ediacaran

Doushantuo Member II

The short interval sampled for Doushantuo Member II (DST II) at Jiuqunao is geochemically similar to the more expanded profile analysed at Jiulongwan (Figs 4 and 5), where no enrichment in redox-sensitive trace-metals, comparable TOC and TS contents, generally anoxic non-sulphidic conditions and mostly positive $\delta^{34}S_{Pyrite}$ values (above 10‰) are found. Previous studies of the Jiulongwan section agree with the present results (Bristow *et al.*, 2009; Li *et al.*, 2010) and suggest that a lack of trace-metal enrichment was a characteristic of the Yangtze Platform during the

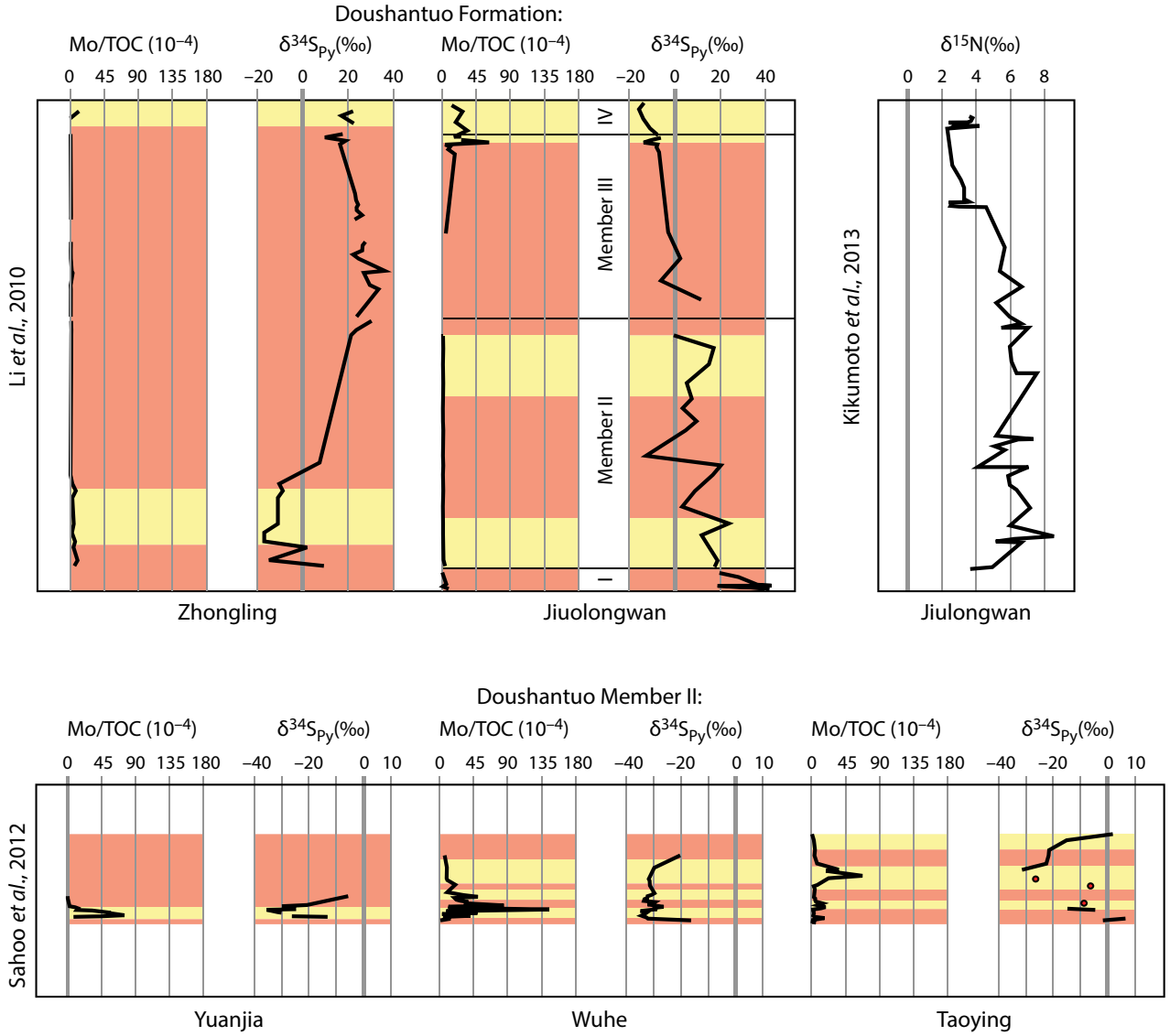

Fig. 14. Other geochemical profiles from previous studies carried out on the Yangtze Platform near the Three Gorges Area (see Fig. 2 for localities). (A) Li *et al.* (2010) and Kikumoto *et al.* (2014) also investigated the Jiulongwan section across the whole Doushantuo Formation and that data confirms the findings of the present study. The Doushantuo Formation at the Zhongling section, *ca* 100 km south of Jiulongwan, exhibits much lower Mo/TOC ratios and a $\delta^{34}S$ profile that mirrors the trend at Jiulongwan up to DST Member II before showing a similarly decreasing trend within DST Members III and IV. (B) Sahoo *et al.* (2012) found elevated Mo/TOC ratios in the DST Member II and generally very low $\delta^{34}S$ values in basinal sections.

deposition of DST II. However, significantly higher enrichments of Mo and V in DST II have been reported from slope and basin sections, where Mo concentrations can attain values from a few tens of ppm (Wallis, 2006; Guo *et al.*, 2007) up to almost 200 ppm (Sahoo *et al.*, 2012). Although there are possible indications of intermittent euxinia in DST II at Jiulongwan, suggested by high Fe_{Py}/Fe_{HR} ratios *ca* 0·7, no Mo enrichment is apparent. Because Mo/TOC and V/TOC ratios remain very low throughout the lower part of the Doushantuo Formation, it is argued here that limited availability of Mo and V in the water column prevailed, at least locally, during deposition of DST II at Jiulongwan.

Independently, palaeogeographic, sedimentological and carbon isotope studies support a rimmed platform margin, which developed soon after deposition of the underlying cap carbonate (Jiang *et al.*, 2011), and the formation of variably

restricted basins on the Yangtze Platform (Jiang *et al.*, 2003b, 2008, 2011; Vernhet, 2007; Vernhet & Reijmer, 2010; Zhu *et al.*, 2013). This suggests that geographic barriers and a lack of access to the open ocean might have controlled trace-metal and sulphate availability from the Early Ediacaran onwards. Furthermore, the $\delta^{34}S$ profiles at Jiulongwan and Jiuqunao are variable but generally enriched in $\delta^{34}S$, possibly resulting from near-quantitative sulphate reduction within a sulphate-poor water column, which is a predictable result of restricted access to the open ocean. Nonetheless, this depends on the isotopic signature of Neoproterozoic sea water sulphate, which, based on sulphate-sulphur isotope studies (see Och & Shields-Zhou, 2012, for a compilation), appears to have been exceptionally high during the Precambrian–Cambrian transition. However, as Li *et al.* (2010) and Sahoo *et al.* (2012) have shown, the sulphur isotopic signature within DST II successions deposited under a euxinic water column on the shelf margin and within the deeper basin exhibit negative excursions between −30‰ and −40‰. Along with high concentrations of redox-sensitive trace-metals (Fig. 14), this indicates enhanced availability of sulphate within the open ocean, resulting in an increased potential for rates of sulphide production to overwhelm the influx of highly reactive Fe, thus leading to euxinic conditions (Poulton & Canfield, 2011) and, hence, extensive trace-metal drawdown. This condition is indicated by low Mo/TOC ratios in DST II on the shelf margin (Li *et al.*, 2010; this study) and greatly elevated Mo/TOC ratios in basinal successions (Sahoo *et al.*, 2012). The nitrogen isotope record of DST II, where most values lie between 3‰ and 6‰ in the Jiulongwan section (see also Kikumoto *et al.*, 2014), and at 6‰ at Jiuqunao section, both representing inner shelf sedimentary successions, indicate that denitrification and nitrogen fixation were well-balanced in the water column, consistent with stable nitrate supply (see also Ader *et al.*, 2014). Together with the above mentioned positive $\delta^{34}S$ signature measured in the Jiulongwan and Jiuqunao sections, this suggests that these successions were deposited in a restricted environment with low sulphate availability but a complete nitrogen cycle within a redox stratified water column.

Doushantuo Member IV (Miaohe)

In the Three Gorges Area, the black shales from the Miaohe Member at Jiulongwan were deposited under euxinic conditions, whereas euxinia is not indicated at Jiuqunao (Figs 4 and 5), which lies *ca* 30 km north-west of the Jiulongwan Formation. Intermittently euxinic conditions are also indicated within the uppermost Doushantuo Formation at Maoshi, which lies *ca* 530 km south-west of the Three Gorges Area in Guizhou Province, suggesting sporadic widespread euxinic conditions on the platform margins during deposition of the upper Doushantuo black shales. While the highest recorded Precambrian Mo concentrations are found at Jiulongwan (>300 ppm; Mo/TOC >180), the Jiuqunao and Maoshi sections exhibit only average shale Mo and V concentrations. In addition, sulphide isotope values are exclusively and distinctively negative in the Miaohe black shale at Jiulongwan, averaging −11·2‰, while at Jiuqunao and Maoshi, mostly positive values were found averaging +18·4‰ and +9·9‰, respectively, with similar trends in both sections (Fig. 11).

Therefore, Doushantuo Member IV (DST IV) at Jiulongwan was deposited under euxinic conditions, with seemingly unrestricted availability of sulphate and redox-sensitive trace-metals. Nitrogen isotopic signatures support stable nitrate availability and suggest that 'normal' marine production helped to fuel euxinia in this case. Hence, because a steady source of nitrate is required, and the present authors can envisage water column stratification, with euxinic bottom waters beneath oxic/dysoxic surface waters. Presumably, oxidized S, N and Mo originated from surface currents that flowed over the lip of the rimmed basin from the open ocean. The Miaohe Member sediments at the Jiuqunao and Maoshi sections, from the Three Gorges Area and Guizhou Province, respectively, do not exhibit any similar enrichment of redox-sensitive trace-metals, while pyrite is enriched in $\delta^{34}S$ (Fig. 11), which suggests that the depositional environment of Jiuqunao and Maoshi could represent more restricted intra-shelf basins that remained isolated from oxygenated surface waters within the inner platform. Because the Jiulongwan and Jiuqunao sections are located close to one another, this finding implies considerable spatial redox complexity within the shelf lagoon.

The nitrogen isotopic signatures of these sections are considerably different: while $\delta^{15}N$ values at Jiulongwan are relatively constant at *ca* 4‰, contrasting end-member $\delta^{15}N$ values are found of *ca* 0·5‰ at Jiuqunao and 6·5‰ at Maoshi. At Jiuqunao, (de)nitrification seems to have been inhibited, possibly due to insufficient availability of nitrate which would also prevent

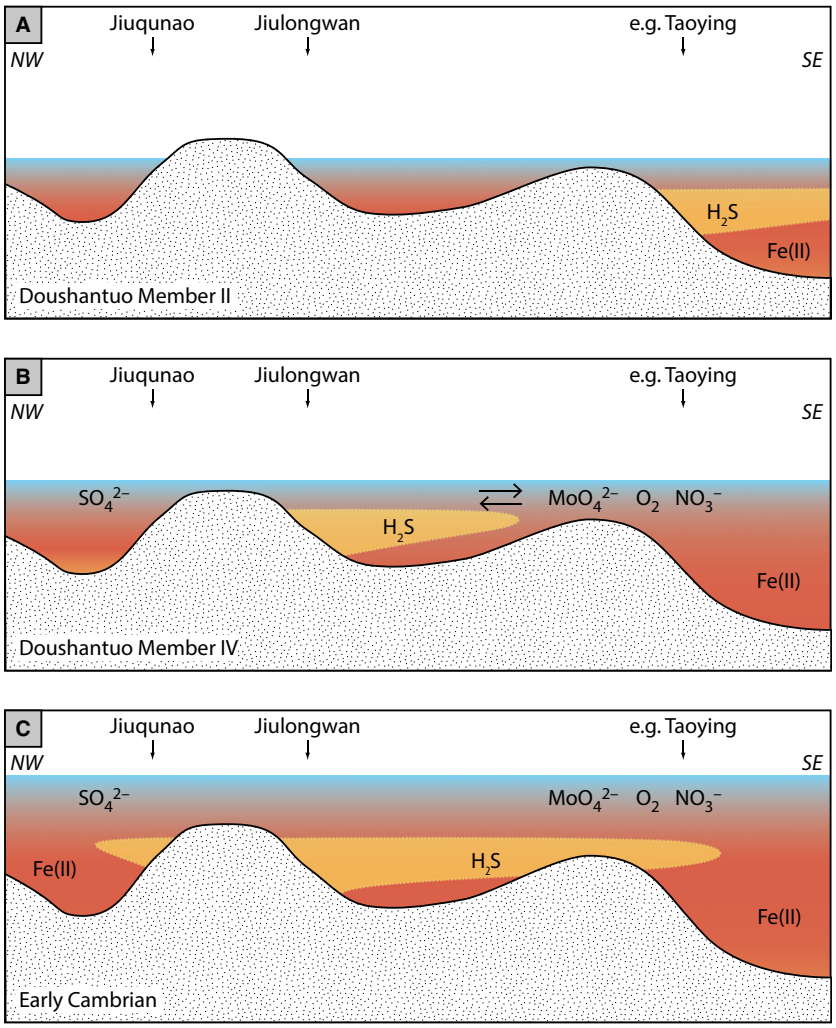

Fig. 15. (A) A restricted intra-shelf basin with a stratified water column including intermittent euxinic conditions such as might have been the case during the deposition of Doushantuo Member II. (B) Schematic illustration of how the Miaohe Member (DST IV) might have been deposited underneath an extended sulphidic wedge due to sea-level rise. The sulphidic wedge, analogous to modern oxygen-minimum zones, has been adopted from Li *et al.* (2010) to account for the very high enrichment in redox-sensitive trace-metals observed at Jiulongwan. (C) With further sea-level rise, the availability of sulphate, along with molybdate, increases in the depositional environment at Jiuqunao and a sulphidic wedge is formed. This schematic illustration is not to scale.

the development of sustained euxinia. In that case, the low $\delta^{15}N$ values indicate that atmospheric nitrogen fixation fuelled productivity after nitrogen loss through organic matter burial. On the other hand, higher values at Maoshi suggest a more balanced nitrogen cycle in a redox stratified water column and the ability to, at least locally, sustain euxinic conditions (Boyle *et al.*, 2013; Cremonese *et al.*, 2013; Ader *et al.*, 2014). Therefore, a gradually increasing exchange with the open ocean can be envisaged, as shown by the transition of pyrite sulphur isotopes from 20‰ to −4‰, in contrast to an average of 18·5‰ at Jiuqunao.

In summary, a rising eustatic sea-level would successively have allowed basins that were restricted or semi-restricted during deposition of DST II to have access to the open ocean, thus increasing the availability of redox-sensitive trace-metals to be scavenged by anoxic and particularly sulphidic bottom waters (Fig. 15). Low sulphate concentrations in the water column during the deposition of DST II were likely to be sufficiently counteracted by overall low Fe(II) concentrations at Jiulongwan, to allow episodic euxinia to develop (Poulton & Canfield, 2011). The euxinic sediments of the Miaohe Member at the Jiulongwan section are accompanied by very high Mo/TOC ratios and negative sulphide isotope values, suggesting a ready supply of redox-sensitive trace-metals and sulphate from the shallow, oxic ocean, probably overlying a sulphidic wedge (Fig. 15), as proposed by Li *et al.* (2010). The apparently close relationship between euxinic conditions and nitrate availability suggests that exchange with the generally oxygenated open ocean was essential to fuel euxinia during times of high productivity, potentially driven by upwelling of P-rich waters. Lower sea-level and basin restriction in these cases may have self-lim-

ited the spread of euxinia by limiting the supply of fixed nitrogen from sources other than microbial nitrogen fixation.

The Baiguoyuan section

Previous studies of the Baiguoyuan section have focussed mainly on the black shale hosted Ag–V ore deposit, generally thought to be of sedimentary-diagenetic origin (Qian *et al.*, 1995; Zhuang *et al.*, 1999). While TOC contents are within the same range as at Jiulongwan, the Miaohe Member at Baiguoyuan is poor in total sulphur (TS; Wallis, 2006). Not surprisingly, although Mo is still slightly enriched at Baiguoyuan with respect to average shale values, Mo concentrations do not exceed a tenth of the maximum content reached at Jiulongwan. On the other hand, V attains concentrations of more than 1 wt% at Baiguoyuan, which is about five times more than the maximum at Jiulongwan (Fig. 4; Wallis, 2006). The depositional environments at Baiguoyuan and Jiulongwan were presumably subject to similar trace-metal availability, but the former was deposited under an anoxic water column where euxinia never developed. Although neither sulphur nor nitrogen isotopic signatures are available for the Baiguoyuan section, it is difficult to formulate a more detailed explanation for the high V concentrations and further research on the section at Baiguoyuan is required. However, at this point these findings merely further corroborate a highly diversified physico-chemical environment on the Yangtze Platform with strongly varying trace-metal availability and redox conditions.

The Early Cambrian

Although the stratigraphic correlation between the Early Cambrian Jiuqunao and Jijiapo successions is not straightforward, peaks in Mo and V enrichment appear to be contemporaneous (Och *et al.*, 2013), especially the prominent peak in Mo concentrations and Mo/TOC ratios observed at the base of the Shuijingtuo Formation (Fig. 11). Maximum Mo and V concentrations are between five and ten times higher within the base of the Shuijingtuo Formation at Jiuqunao compared with Jijiapo, but while V contents return to values close to average shale (e.g. McLennan, 2001), Mo decreases to values still significantly higher than average shale. One explanation is that euxinia only marginally developed during the deposition of the Shuijingtuo black shale at Jijiapo but was pronounced at Jiuqunao, which is supported by iron speciation data. However, the $\delta^{34}S$ excursion around the Yangjiahe/Shuijingtuo boundary at Jijiapo section, where a euxinic interval is observed, does not seem to have led to the scavenging of trace-metals. The Mo enrichment only occurs above this interval, along with a significant decrease in $\delta^{34}S$. This indicates that higher sulphate concentrations were necessary to fuel sufficient sulphide production to draw down Mo. Because euxinic conditions are not indicated, it is likely that Mo precipitated during very early diagenesis close to the sediment–water interface. In addition, elevated sulphate concentrations probably coincided with higher molybdate concentrations in the water column.

The Mo and V profiles from the Huanglian and Longbizui sections, deposited in the basin, exhibit a peak around the Precambrian–Cambrian boundary, comparable to that observed at Jiuqunao and Jijiapo (Figs 11 and 12). Hence, the present authors suggest that both environments experienced similar ocean chemistry, possibly due to further eustatic sea-level rise, which allowed for a connection between the deeper basin and the previously intra-shelf basins (e.g. Haq & Schutter, 2008). The predominantly high sulphur isotope values from Longbizui, however, may suggest a certain degree of sulphate limitation in the water column. Minimum $\delta^{34}S$ values correlate with euxinic sediments and indicate that increases in oceanic sulphate concentrations may have intensified the production of H_2S. A prominent geochemical feature at the Xiaotan section, which was deposited further inside the Yangtze Platform, is the possibility that the water column might have experienced oxic conditions above the last analysed black shale layer during deposition of the Yuanshan Formation (Fig. 13; Och *et al.*, 2013). Moreover, $\delta^{15}N$ stabilizes at values *ca* 2·5‰, recovering from values between 0‰ and 2‰ found within the anoxic-ferruginous interval (Cremonese *et al.*, 2013).

Although merely based on scarce data, the nitrogen isotope signatures at Jijiapo, Jiuqunao and Longbizui exhibit their lowest values within the black shales deposited under euxinic conditions, which is in accordance with the model of Boyle *et al.* (2013), who hypothesized that euxinia should correlate with nitrogen fixation and low, atmospheric nitrogen isotope values (at least in the Precambrian; cf. Godfrey *et al.*, 2013). In the Ediacaran section discussed above (for example, the black shales of DST IV at Jiulongwan), this was not the case. It appears that

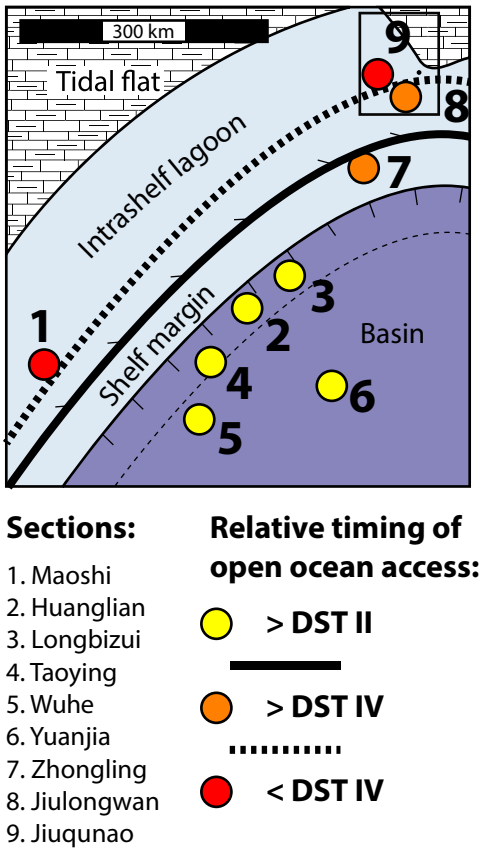

Fig. 16. Schematic configuration of the Yangtze Platform margin across the Precambrian–Cambrian transition with the locations of the sections analysed from the present study and the literature (Li *et al.*, 2010; Sahoo *et al.*, 2012). The yellow filled circles represent basinal sedimentary successions with access to the open ocean since the deposition of the Lower Doushantuo Formation (DST Member II), which exhibit the earliest Mo enrichment in Earth history (Sahoo *et al.*, 2012) and might pinpoint the emergence of a widely oxygenated Earth surface. The orange filled circles indicate the sections with onset of trace-metal enrichment occurring during the sedimentation of the Upper Doushantuo Formation (Miaohe Member) whereas the red filled circles show the locations of sedimentary basins where the trace-metal and sulphate availability only increased during the Early Cambrian.

the main difference between periods of euxinic environments in the Ediacaran and the Cambrian on the Yangtze Platform is that euxinia was less widespread and pervasive during deposition of the Doushantuo Formation, when it was established in the form of a sulphidic wedge in upwelling areas, carrying over in places to distal shelf lagoon areas such as Jiulongwan (Li *et al.*, 2010). During the Early Cambrian, on the other hand, euxinic conditions have been reported from both basin and platform sections (Canfield *et al.*, 2008; Och *et al.*, 2013, and references therein). At Jiuqunao and Jijiapo (Figs 9 and 10), after the positive peak in Mo and V, nitrogen isotopic signatures decrease to values between 0‰ and −1‰, consistent with an increase in N_2-fixation and/or photic zone anoxia, possibly facilitated by high concentrations of nitrogenase co-factors (Mo and V) (e.g. Canfield *et al.*, 2010b; Zhang *et al.*, 2014); N_2-fixation could then have contributed significantly to the increase in primary productivity, sustaining anoxia and sulphidic conditions. These features can also be observed at Jiuqunao and Jijiapo, although to a different extent due to the different palaeogeographic settings. Nevertheless, Mo and V peaks seem to be widespread on the Yangtze Platform, and the increase in bio-available Mo and V, in a dominantly ferruginous ocean might have triggered unprecedented primary production and organic matter delivery to the ocean floor (Anbar & Knoll, 2002), which created conditions favourable for intensified sulphate reduction and the emergence of widespread and sustained euxinia in the Early Cambrian, prior to the Cambrian bioradiation.

The effects on ecosystems of changing spatial redox distribution

It has been established that many extant animals are facultative anaerobes and so are not wholly dependent on oxygen (Martin & Müller, 2007; Budd, 2008); some are even able to withstand sulphidic conditions throughout their life cycle (Danovaro *et al.*, 2010). Nonetheless, motility and other muscular activities of animals are repressed at low oxygen levels. Therefore, the finding of widespread anoxia and spatially extensive euxinia across the Ediacaran–Cambrian boundary seems to be incompatible with the ongoing Cambrian explosion, which is commonly believed to have been triggered by oceanic, and possibly atmospheric, oxygenation. One consequence of such spatial variability in redox conditions would be to create dynamically changing benthic ecosystems. Although preliminary, the present results may help to shed light on the distribution of benthic and, to a lesser extent, pelagic ecosystems on the Yangtze Platform. The most famous Ediacaran fronds are indisputably benthic but have only been reported in China from the Shibantan Member of the Dengying Formation, which is constrained

by Fe speciation and rare earth element (REE) distributions to have been deposited under largely oxygenated conditions (Ling *et al.*, 2013; Duda *et al.*, 2014); this is supported by examples of both body and trace fossils (Chen *et al.*, 2013). As shown above, more distal equivalents such as the Liuchapo Formation, which are largely devoid of any diagnostic fossils, were deposited under anoxic and in some cases even euxinic conditions, thus restricting benthic ecosystems at this time to the generally shallower, inner Yangtze Platform.

The Miaohe biota (Steiner, 1994; Ding *et al.*, 1996) is widely known but generally limited to just a few sections from the inner shelf lagoons close to the Jiuqunao section (the Miaohe section is *ca* 1 km distant and lithologically very similar) and Maoshi section (Guizhou Province). No Miaohe fossil assemblage has been reported from the equivalent horizon at the Jiulongwan section, which according to the present data experienced persistent sulphidic conditions. One possible interpretation of this is that dissolved sulphide was toxic to the Miaohe biota.

CONCLUSIONS

The multi-proxy approach, including the redox-sensitive trace-metals Mo and V, iron speciation, sulphide and nitrogen isotopes suggest a gradually increasing number of intra-shelf basins on the Yangtze Platform gaining access to the greater availability of trace-metals and sulphate present in the open ocean (Fig. 16). This effect can best be illustrated at the sections around Jiulongwan, where sea-level rise submerged the previously restricted rimmed basin during deposition of the Miaohe Member of the Doushantuo Formation. There, Mo/TOC ratios suggest good communication with the open ocean, while the combination of Fe speciation and S isotopes suggests that euxinic conditions did not limit sulphate (or nitrate) availability. Although it is likely that the trace-metal and sulphate inventory increased gradually during the Precambrian–Cambrian transition, the present authors suggest that changing sea-level played an important role in the expression of the Neoproterozoic Oxygenation Event (NOE) at continental margins. However, although the change in biogeochemical cycling across this large transitional time interval follows a clear trend, the details rely on the current stratigraphic framework that may change with additional age constraints, and the signature of changing ocean chemistry and bathymetry cannot clearly be separated at present.

The apparent switch in nitrogen cycling, whereby $\delta^{15}N$ values remained heavy during sulphidic periods in the Ediacaran, but with light values during euxinia in the Early Cambrian, possibly arises from sulphidic conditions being confined to sulphidic wedges in the upwelling areas during the Ediacaran. In contrast, productivity and subsequent sulphate reduction was probably fuelled by the nitrate reservoir of the open ocean during the early Cambrian. In the Early Cambrian, more widespread euxinic conditions across flooded shelves precluded incomplete denitrification, leading to lower $\delta^{15}N$ values. A highly dynamic environment, both bathymetrically and chemically, including a trend to higher oxygen concentrations in the ocean interrupted by regional euxinic events, might have spurred on the emergence and diversification of animals for which the fossil record of the Cambrian Explosion can only represent a glimpse.

ACKNOWLEDGEMENTS

This study was initiated through the funding from the German Research Foundation (DFG, FOR 736), and continued through NERC grant NE/I005978/1, whereby the extensive fieldwork was mainly supported by the National Basic Research Program of China (2013CB835000) and the Natural Science Foundation of China (NSFC). We are very grateful to Tony Osborn from the Wolfson Laboratory at UCL, Alison McAnena from Newcastle University, Artur Fugmann from the WWU-Muenster, and Heizhen Wei from Nanjing University for their expert and invaluable assistance in the laboratory. In addition, we owe great thanks to Magali Ader and Ganqing Jiang for reviewing this manuscript in an insightful and constructive way.

REFERENCES

Ader, M., **Sansjofre, P.**, **Halverson, G.P.**, **Busigny, V.**, **Trindade, R.I.F.**, **Kunzmann, M.** and **Nogueira, A.C.R.** (2014) Ocean redox structure across the Late Neoproterozoic oxygenation event: a nitrogen isotope perspective. *Earth Planet. Sci. Lett.*, **396**, 1–13.

Algeo, T.J. and **Lyons, T.W.** (2006) Mo-total organic carbon covariation in modern anoxic marine environments:

implications for analysis of paleoredox and paleohydrographic conditions. *Paleoceanography* **21**.

Anbar, A.D. (2004) Molybdenum stable isotopes: observations, interpretations and directions. *Rev. Mineral. Geochem.*, **55**(1), 429–454.

Anbar, A.D. and **Knoll, A.H.** (2002) Proterozoic ocean chemistry and evolution: a bioinorganic bridge? *Science*, **297**, 1137–1142.

Archer, C. and **Vance, D.** (2006) Coupled Fe and S isotope evidence for Archean microbial Fe(III) and sulfate reduction. *Geology*, **34**, 153–156.

Arnold, G.L., **Anbar, A.D.**, **Barling, J.** and **Lyons, T.W.** (2004) Molybdenum isotope evidence for widespread anoxia in mid-Proterozoic oceans. *Science*, **304**, 87–90.

Babcock, L.E. and **Peng, S.** (2007) Cambrian chronostratigraphy: current state and future plans. *Palaeogeogr. Palaeoclimatol. Palaeoecol.*, **254**, 62–66.

Babcock, L.E., **Zhang, W.** and **Leslie, S.A.** (2001) The Chengjiang Biota: record of the Early Cambrian diversification of life and clues to exceptional preservation of fossils. *GSA Today*, **11**, 4–9.

Bekker, A., **Holland, H.D.**, **Wang, P.-L.**, **Rumble, D., III**, **Stein, H.J.**, **Hannah, J.L.**, **Coetzee, L.L.** and **Beukes, N.J.** (2004) Dating the rise of atmospheric oxygen. *Nature*, **427**, 117–120.

Bertine, K.K. and **Turekian, K.K.** (1973) Molybdenum in marine deposits. *Geochim. Cosmochim. Acta*, **37**, 1415–1434.

Boyle, R.A., **Clark, J.R.**, **Poulton, S.W.**, **Shields-Zhou, G.**, **Canfield, D.E.** and **Lenton, T.M.** (2013) Nitrogen cycle feedbacks as a control on euxinia in the mid-Proterozoic ocean. *Nat. Commun.*, **4**, 1–10.

Brandes, J.A. and **Devol, A.H.** (2002) A global marine-fixed nitrogen isotopic budget: implications for Holocene nitrogen cycling. *Global Biogeochem. Cycles*, **16**, 1120.

Brasier, M., **Cowie, J.** and **Taylor, M.** (1994) Decision on the Precambrian-Cambrian boundary stratotype. *Episodes*, **17**, 3–8.

Breit, G.N. and **Wanty, R.B.** (1991) Vanadium accumulation in carbonaceous rocks: a review of geochemical controls during deposition and diagenesis. *Chem. Geol.*, **91**(2), 83–97.

Bristow, T.F., **Kennedy, M.J.**, **Derkowski, A.**, **Droser, M.L.**, **Jiang, G.** and **Creaser, R.A.** (2009) Mineralogical constraints on the paleoenvironments of the Ediacaran Doushantuo Formation. *Proc. Natl Acad. Sci.*, **106**, 13190–13195.

Brocks, J.J., **Logan, G.A.**, **Buick, R.** and **Summons, R.E.** (1999) Archean molecular fossils and the early rise of eukaryotes. *Science*, **285**, 1033–1036.

Brocks, J.J., **Love, G.D.**, **Summons, R.E.**, **Knoll, A.H.**, **Logan, G.A.** and **Bowden, S.A.** (2005) Biomarker evidence for green and purple sulphur bacteria in a stratified Palaeoproterozoic sea. *Nature*, **437**, 866–870.

Broecker, W.S. and **Peng, T.H.** (1982) *Tracers in the Sea*. Eldigio Press, Columbia University, Palisades, NY.

Budd, G.E. (2008) The earliest fossil record of the animals and its significance. *Phil. Trans. Roy. Soc. B Biol. Sci.*, **363**, 1425–1434.

Calvert, S.E. and **Piper, D.Z.** (1984) Geochemistry of ferromanganese nodules from DOMES site a, Northern Equatorial Pacific: multiple diagenetic metal sources in the deep sea. *Geochim. Cosmochim. Acta*, **48**, 1913–1928.

Campbell, I.H. and **Allen, C.M.** (2008) Formation of supercontinents linked to increases in atmospheric oxygen. *Nat. Geosci.*, **1**, 554–558.

Canfield, D.E. (1998) A new model for Proterozoic ocean chemistry. *Nature*, **396**, 450–453.

Canfield, D.E. (2001) Biogeochemistry of sulfur isotopes. *Rev. Mineral. Geochem.*, **43**, 607–636.

Canfield, D.E. (2005) The early history of atmospheric oxygen: homage to Robert M. Garrels. *Annu. Rev. Earth Planet. Sci.*, **33**, 1–36.

Canfield, D.E. and **Raiswell, R.** (1999) The evolution of the sulfur cycle. *Am. J. Sci.*, **299**, 697–723.

Canfield, D.E. and **Teske, A.** (1996) Late Proterozoic rise in atmospheric oxygen concentration inferred from phylogenetic and sulphur-isotope studies. *Nature*, **382**, 127–132.

Canfield, D.E., **Lyons, T.W.** and **Raiswell, R.** (1996) A model for iron deposition to euxinic Black Sea sediments. *Am. J. Sci.*, **296**, 818–834.

Canfield, D.E., **Raiswell, R.**, **Westrich, J.T.**, **Reaves, C.M.** and **Berner, R.A.** (1986) The use of chromium reduction in the analysis of reduced inorganic sulfur in sediments and shales. *Chem. Geol.*, **54**, 149–155.

Canfield, D.E., **Poulton, S.W.** and **Narbonne, G.M.** (2007) Late-Neoproterozoic deep-ocean oxygenation and the rise of animal life. *Science*, **315**, 92–95.

Canfield, D.E., **Poulton, S.W.**, **Knoll, A.H.**, **Narbonne, G.M.**, **Ross, G.**, **Goldberg, T.** and **Strauss, H.** (2008) Ferruginous conditions dominated later Neoproterozoic deep-water chemistry. *Science*, **321**, 949–952.

Canfield, D.E., **Farquhar, J.** and **Zerkle, A.L.** (2010a) High isotope fractionations during sulfate reduction in a low-sulfate euxinic ocean analog. *Geology*, **38**, 415–418.

Canfield, D.E., **Glazer, A.N.** and **Falkowski, P.G.** (2010b) The evolution and future of earth's nitrogen cycle. *Science*, **330**, 192–196.

Chang, H., **Chu, X.**, **Feng, L.** and **Huang, J.** (2009) Terminal Ediacaran anoxia in deep-ocean: trace element evidence from cherts of the Liuchapo Formation, South China. *Sci. China Ser. Earth Sci.*, **52**, 807–822.

Chen, Z., **Zhou, C.**, **Meyer, M.**, **Xiang, K.**, **Schiffbauer, J.D.**, **Yuan, X.** and **Xiao, S.** (2013) Trace fossil evidence for Ediacaran bilaterian animals with complex behaviors. *Precambrian Res.*, **224**, 690–701.

Cloud, P. (1972) A working model of the primitive Earth. *Am. J. Sci.*, **272**, 537–548.

Collier, R.W. (1985) Molybdenum in the Northeast Pacific Ocean. *Limnol. Oceanogr.*, **30**, 1351–1354.

Collier, R. and **Edmond, J.** (1984) The trace element geochemistry of marine biogenic particulate matter. *Prog. Oceanogr.*, **13**, 113–199.

Compston, W., **Williams, I.S.**, **Kirschvink, J.L.**, **Zichao, Z.** and **Guogan, M.A.** (1992) Zircon U-Pb ages for the Early Cambrian time-scale. *J. Geol. Soc.*, **149**, 171–184.

Compston, W., **Zhang, Z.**, **Cooper, J.A.**, **Ma, G.** and **Jenkins, R.J.F.** (2008) Further SHRIMP geochronology on the early Cambrian of South China. *Am. J. Sci.*, **308**, 399–420.

Condon, D., **Zhu, M.**, **Bowring, S.**, **Wang, W.**, **Yang, A.** and **Jin, Y.** (2005) U-Pb Ages from the Neoproterozoic Doushantuo Formation, China. *Science*, **308**, 95–98.

Cowie, J. (1985) Continuing work on the Precambrian-Cambrian boundary. *Episodes*, **8**, 93–97.

Cremonese, L., **Shields-Zhou, G.**, **Struck, U.**, **Ling, H.-F.**, **Och, L.**, **Chen, X.** and **Li, D.** (2013) Marine biogeochemical cycling during the early Cambrian constrained by a nitrogen and organic carbon isotope study of the Xiaotan section, South China. *Precambrian Res.*, **225**, 148–165.

Cremonese, L., **Shields-Zhou, G.A.**, **Struck, U.**, **Ling, H.-F.** and **Och, L.M.** (2014) Nitrogen and organic carbon isotope stratigraphy of the Yangtze Platform during the Ediacaran-

Cambrian transition in South China. *Palaeogeogr. Palaeoclimatol. Palaeoecol.*, **398**, 165–186.

Crusius, J., **Calvert, S.**, **Pedersen, T.** and **Sage, D.** (1996) Rhenium and molybdenum enrichments in sediments as indicators of oxic, suboxic and sulfidic conditions of deposition. *Earth Planet. Sci. Lett.*, **145**, 65–78.

Cui, H., **Kaufman, A.J.**, **Xiao, S.**, **Zhu, M.**, **Zhou, C.** and **Liu, X.-M.** (2015) Redox architecture of an Ediacaran ocean margin: integrated chemostratigraphic (δ13C–δ34S–87Sr/86Sr–Ce/Ce*) correlation of the Doushantuo Formation, South China. *Chem. Geol.*, **405**, 48–62.

Danovaro, R., **Dell'Anno, A.**, **Pusceddu, A.**, **Gambi, C.**, **Heiner, I.** and **Kristensen, R.M**. (2010) The first metazoa living in permanently anoxic conditions. *BMC Biol.* **8**: 30.

Derry, L.A., **Kaufman, A.J.** and **Jacobsen, S.B.** (1992) Sedimentary cycling and environmental-change in the Late Proterozoic – evidence from stable and radiogenic isotopes. *Geochim. Cosmochim. Acta*, **56**, 1317–1329.

Des Marais, D.J., **Strauss, H.**, **Summons, R.E.** and **Hayes, J.M.** (1992) Carbon isotope evidence for the stepwise oxidation of the Proterozoic environment. *Nature*, **359**, 605–609.

Ding, L., **Zhang, L.**, **Li, Y.** and **Dong, J.** (1992) *The Study of the Late Sinian-Early Cambrian Biotas from the Northern Margin of the Yangtze Platform*. Scientific and Technical Documents Publishing House, Beijing, 135 pp.

Ding, L., **Li, Y.**, **Hu, X.**, **Xiao, Y.**, **Su, C.** and **Huang, J.** (1996) *Sinian Miaohe Biota*. Geological Publishing House, Beijing.

Duda, J.-P., **Blumenberg, M.**, **Thiel, V.**, **Simon, K.**, **Zhu, M.** and **Reitner, J.** (2014) Geobiology of a palaeoecosystem with Ediacara-type fossils: the Shibantan Member (Dengying Formation, South China). *Precambrian Res.*, **255** Part 1, 48–62.

Eady, R.R. (2003) Current status of structure function relationships of vanadium nitrogenase. *Coord. Chem. Rev.*, **237**, 23–30.

Erickson, B.E. and **Helz, G.R.** (2000) Molybdenum(VI) speciation in sulfidic waters: stability and lability of thiomolybdates. *Geochim. Cosmochim. Acta*, **64**, 1149–1158.

Frei, R., **Gaucher, C.**, **Poulton, S.W.** and **Canfield, D.E.** (2009) Fluctuations in Precambrian atmospheric oxygenation recorded by chromium isotopes. *Nature*, **461**, 250–253.

Gill, B.C., **Lyons, T.W.**, **Young, S.A.**, **Kump, L.R.**, **Knoll, A.H.** and **Saltzman, M.R.** (2011) Geochemical evidence for widespread euxinia in the Later Cambrian ocean. *Nature*, **469**, 80–83.

Godfrey, L.V., **Poulton, S.W.**, **Bebout, G.E.** and **Fralick, P.W.** (2013) Stability of the nitrogen cycle during development of sulfidic water in the redox-stratified late Paleoproterozoic Ocean. *Geology*, **41**, 655–658.

Goldberg, T., **Archer, C.**, **Vance, D.**, **Thamdrup, B.**, **McAnena, A.** and **Poulton, S.W**. (2012) Controls on Mo isotope fractionations in a Mn-rich anoxic marine sediment, Gullmar Fjord, Sweden. *Chem. Geol.*, **296–297**, 73–82.

Guo, Q., **Shields, G.A.**, **Liu, C.**, **Strauss, H.**, **Zhu, M.**, **Pi, D.**, **Goldberg, T.** and **Yang, X.** (2007) Trace element chemostratigraphy of two Ediacaran-Cambrian successions in South China: implications for organosedimentary metal enrichment and silicification in the Early Cambrian. *Palaeogeogr. Palaeoclim. Palaeoecol.*, **254**, 194–216.

Habicht, K.S., **Gade, M.**, **Thamdrup, B.**, **Berg, P.** and **Canfield, D.E.** (2002) Calibration of sulfate levels in the Archean Ocean. *Science*, **298**, 2372–2374.

Hagadorn, J.W. (2002) Chengjiang: early record of the Cambrian explosion. In: *Exceptional Fossil Preservation: A Unique View on the Evolution of Marine Life* (Eds D.J. Bottjer, W. Etter, J.W. Hagadorn and C.M. Tang), pp. 35–60. Columbia University Press, New York, NY.

Haq, B.U. and **Schutter, S.R.** (2008) A chronology of Paleozoic sea-level changes. *Science*, **322**, 64–68.

Harrison, A.G. and **Thode, H.G.** (1958) Mechanism of the bacterial reduction of sulphate from isotope fractionation studies. *Trans. Faraday Soc.*, **54**, 84–92.

Helz, G.R., **Miller, C.V.**, **Charnock, J.M.**, **Mosselmans, J.F.W.**, **Pattrick, R.A.D.**, **Garner, C.D.** and **Vaughan, D.J.** (1996) Mechanism of molybdenum removal from the sea and its concentration in black shales: EXAFS evidence. *Geochim. Cosmochim. Acta*, **60**, 3631–3642.

Helz, G.R., **Bura-Nakic, E.**, **Mikac, N.** and **Ciglenecki, I.** (2011) New model for molybdenum behavior in euxinic waters. *Chem. Geol.*, **284**, 323–332.

Higgins, M.B., **Robinson, R.S.**, **Husson, J.M.**, **Carter, S.J.** and **Pearson, A.** (2012) Dominant eukaryotic export production during ocean anoxic events reflects the importance of recycled NH4+. *Proc. Natl Acad. Sci. USA* **109**, 2269–2274.

Ho, T.-Y., **Quigg, A.**, **Finkel, Z.V.**, **Milligan, A.J.**, **Wyman, K.**, **Falkowski, P.G.** and **Morel, F.M.M.** (2003) The elemental composition of some marine phytoplankton. *J. Phycol.*, **39**, 1145–1159.

Hoffman, P.F., **Kaufman, A.J.**, **Halverson, G.P.** and **Schrag, D.P.** (1998) A Neoproterozoic snowball earth. *Science*, **281**, 1342–1346.

Hoffman, P.F., **Halverson, G.P.**, **Domack, E.W.**, **Husson, J.M.**, **Higgins, J.A.** and **Schrag, D.P.** (2007) Are basal Ediacaran (635 Ma) post-glacial "cap dolostones" diachronous? *Earth Planet. Sci. Lett.*, **258**, 114–131.

Holland, H.D. (1984) *The Chemical Evolution of the Atmosphere and Oceans*. Princeton University Press, Princeton, NY, 582 pp.

Holland, H.D. (2002) Volcanic gases, black smokers, and the great oxidation event. *Geochim. Cosmochim. Acta*, **66**, 3811–3826.

Holland, H.D. (2006) The oxygenation of the atmosphere and oceans. *Phil. Trans. Roy. Soc. B Biol. Sci.*, **361**, 903–915.

Ishikawa, T., **Ueno, Y.**, **Komiya, T.**, **Sawaki, Y.**, **Han, J.**, **Shu, D.**, **Li, Y.**, **Maruyama, S.** and **Yoshida, N.** (2008) Carbon isotope chemostratigraphy of a Precambrian/Cambrian boundary section in the Three Gorge area, South China: prominent global-scale isotope excursions just before the Cambrian explosion. *Gondwana Res.*, **14**, 193–208.

Isley, A.E. and **Abbott, D.H.** (1999) Plume-related mafic volcanism and the deposition of banded iron formation. *J. Geophys. Res.*, **104**(461–415), 477.

Jenkins, R.J.F., **Cooper, J.A.** and **Compston, W.** (2002) Age and biostratigraphy of Early Cambrian tuffs from SE Australia and southern China. *J. Geol. Soc.*, **159**, 645–658.

Jiang, G., **Kennedy, M.J.** and **Christie-Blick, N.** (2003a) Stable isotopic evidence for methane seeps in Neoproterozoic postglacial cap carbonates. *Nature*, **426**, 822–826.

Jiang, G., **Sohl, L.E.** and **Christie-Blick, N.** (2003b) Neoproterozoic stratigraphic comparison of the Lesser Himalaya (India) and Yangtze block (south China): paleogeographic implications. *Geology*, **31**, 917–920.

Jiang, G., **Kennedy, M.J.**, **Christie-Blick, N.**, **Wu, H.** and **Zhang, S.** (2006) Stratigraphy, sedimentary structures, and textures of the Late Neoproterozoic Doushantuo Cap carbonate in South China. *J. Sed. Res.*, **76**, 978–995.

Jiang, G., **Kaufman, A.J.**, **Christie-Blick, N.**, **Zhang, S.** and **Wu, H.** (2007) Carbon isotope variability across the Ediacaran Yangtze platform in South China: implications for a large surface-to-deep ocean $\delta^{13}C$ gradient. *Earth Planet. Sci. Lett.*, **261**, 303–320.

Jiang, G., **Zhang, S.**, **Shi, X.** and **Wang, X.** (2008) Chemocline instability and isotope variations of the Ediacaran Doushantuo basin in South China. *Sci. China, Ser. D Earth Sci.*, **51**, 1560–1569.

Jiang, S.-Y., **Pi, D.-H.**, **Heubeck, C.**, **Frimmel, H.**, **Liu, Y.-P.**, **Deng, H.-L.**, **Ling, H.-F.** and **Yang, J.-H.** (2009) Early Cambrian ocean anoxia in South China. *Nature*, **459**, E5–E6.

Jiang, G., **Shi, X.**, **Zhang, S.**, **Wang, Y.** and **Xiao, S.** (2011) Stratigraphy and paleogeography of the Ediacaran Doushantuo Formation (ca. 635-551 Ma) in South China. *Gondwana Res.*, **19**, 831–849.

Johnston, D.T., **Farquhar, J.**, **Wing, B.A.**, **Kaufman, A.J.**, **Canfield, D.E.** and **Habicht, K.S.** (2005) Multiple sulfur isotope fractionations in biological systems: a case study with sulfate reducers and sulfur disproportionators. *Am. J. Sci.*, **305**, 645–660.

Johnston, D.T., **Wolfe-Simon, F.**, **Pearson, A.** and **Knoll, A.H.** (2009) Anoxygenic photosynthesis modulated Proterozoic oxygen and sustained Earth's middle age. *Proc. Natl Acad. Sci.*, **106**, 16925–16929.

Jones, G.E. and **Starkey, R.L.** (1957) Fractionation of stable isotopes of sulfur by microorganisms and their role in deposition of native sulfur. *Appl. Environ. Microbiol.*, **5**, 111–118.

Kaplan, I.R. and **Rittenberg, S.C.** (1964) Microbiological fractionation of sulphur isotopes. *J. Gen. Microbiol.*, **34**, 195–212.

Kasting, J.F. and **Ono, S.** (2006) Palaeoclimates: the first two billion years. *Phil. Trans. Roy. Soc. B Biol. Sci.*, **361**, 917–929.

Kemp, A.L.W. and **Thode, H.G.** (1968) The mechanism of the bacterial reduction of sulphate and of sulphite from isotope fractionation studies. *Geochim. Cosmochim. Acta*, **32**, 71–91.

Kendall, B., **Reinhard, C.T.**, **Lyons, T.W.**, **Kaufman, A.J.**, **Poulton, S.W.** and **Anbar, A.D.** (2010) Pervasive oxygenation along late Archaean ocean margins. *Nat. Geosci.*, **3**, 647–652.

Kikumoto, R., **Tahata, M.**, **Nishizawa, M.**, **Sawaki, Y.**, **Maruyama, S.**, **Shu, D.**, **Han, J.**, **Komiya, T.**, **Takai, K.** and **Ueno, Y.** (2014) Nitrogen isotope chemostratigraphy of the Ediacaran and Early Cambrian platform sequence at three Gorges, South China. *Gondwana Res.*, **25**, 1057–1069.

Kirschvink, J.L., **Gaidos, E.J.**, **Bertani, L.E.**, **Beukes, N.J.**, **Gutzmer, J.**, **Maepa, L.N.** and **Steinberger, R.E.** (2000) Paleoproterozoic snowball earth: extreme climatic and geochemical global change and its biological consequences. *Proc. Natl Acad. Sci. USA*, **97**, 1400–1405.

Knoll, A.H., **Javaux, E.J.**, **Hewitt, D.** and **Cohen, P.** (2006) Eukaryotic organisms in Proterozoic oceans. *Phil. Trans. Roy. Soc. B Biol. Sci.*, **361**, 1023–1038.

Landing, E. (1994) Precambrian-Cambrian boundary global stratotype ratified and a new perspective of Cambrian time. *Geology*, **22**, 179–182.

Le Guerroué, E., **Allen, P.A.**, **Cozzi, A.**, **Etienne, J.L.** and **Fanning, M.** (2006) 50Myr recovery from the largest negative $\delta^{13}C$ excursion in the Ediacaran ocean. *Terra Nova*, **18**, 147–153.

Li, Z.-X., **Zhang, L.** and **Powell, C.M.** (1995) South China in Rodinia: part of the missing link between Australia-East Antarctica and Laurentia? *Geology*, **23**, 407–410.

Li, Z.X., **Li, X.H.**, **Kinny, P.D.** and **Wang, J.** (1999) The breakup of Rodinia: did it start with a mantle plume beneath South China? *Earth Planet. Sci. Lett.*, **173**, 171–181.

Li, Z.X., **Li, X.H.**, **Zhou, H.** and **Kinny, P.D.** (2002) Grenvillian continental collision in south China: new SHRIMP U-Pb zircon results and implications for the configuration of Rodinia. *Geology*, **30**, 163–166.

Li, X.H., **Li, Z.X.**, **Ge, W.**, **Zhou, H.**, **Li, W.**, **Liu, Y.** and **Wingate, M.T.D.** (2003a) Neoproterozoic granitoids in South China: crustal melting above a mantle plume at ca. 825 Ma? *Precambrian Res.*, **122**, 45–83.

Li, Z.X., **Li, X.H.**, **Kinny, P.D.**, **Wang, J.**, **Zhang, S.** and **Zhou, H.** (2003b) Geochronology of Neoproterozoic syn-rift magmatism in the Yangtze Craton, South China and correlations with other continents: evidence for a mantle superplume that broke up Rodinia. *Precambrian Res.*, **122**, 85–109.

Li, W.-X., **Li, X.-H.** and **Li, Z.-X.** (2005) Neoproterozoic bimodal magmatism in the Cathaysia Block of South China and its tectonic significance. *Precambrian Res.*, **136**, 51–66.

Li, C., **Love, G.D.**, **Lyons, T.W.**, **Fike, D.A.**, **Sessions, A.L.** and **Chu, X.** (2010) A stratified redox model for the Ediacaran ocean. *Science*, **328**, 80–83.

Li, D., **Ling, H.-F.**, **Shields-Zhou, G.A.**, **Chen, X.**, **Cremonese, L.**, **Och, L.**, **Thirlwall, M.** and **Manning, C.J.** (2013) Carbon and strontium isotope evolution of seawater across the Ediacaran-Cambrian transition: evidence from the Xiaotan section, NE Yunnan, South China. *Precambrian Res.*, **225**, 128–147.

Ling, H.F., **Feng, H.Z.**, **Pan, J.Y.**, **Jiang, S.Y.**, **Chen, Y.Q.** and **Chen, X.** (2007) Carbon isotope variation through the Neoproterozoic Doushantuo and Dengying Formations, South China: implications for chemostratigraphy and paleoenvironmental change. *Palaeogeogr. Palaeoclimatol. Palaeoecol.*, **254**, 158–174.

Ling, H.-F., **Chen, X.**, **Li, D.**, **Wang, D.**, **Shields-Zhou, G.A.** and **Zhu, M.** (2013) Cerium anomaly variations in Ediacaran–earliest Cambrian carbonates from the Yangtze Gorges area, South China: implications for oxygenation of coeval shallow seawater. *Precambrian Res.*, **225**, 110–127.

Lu, M., **Zhu, M.**, **Zhang, J.**, **Shields-Zhou, G.**, **Li, G.**, **Zhao, F.**, **Zhao, X.** and **Zhao, M.** (2013) The DOUNCE event at the top of the Ediacaran Doushantuo Formation, South China: broad stratigraphic occurrence and non-diagenetic origin. *Precambrian Res.*, **225**, 86–109.

Luo, H., **Jiang, Z.**, **Wu, X.**, **Lin, O.**, **Song, X.** and **Xue, X.** (1992) A further research on the Precambrian-Cambrian boundary at Meishucun section of Jinning, Yunnan, China. *Acta Geol. Sinica*, **5**, 197–207.

Lyons, T.W. and **Gill, B.C.** (2010) Ancient sulfur cycling and oxygenation of the early biosphere. *Elements* **6**, 93–99.

Martin, W.F. and Müller, M. (eds) (2007) *Origin of Mitochondria and Hydrogenosomes*. Springer, Heidelberg, Germany.

März, C., **Poulton, S.W.**, **Beckmann, B.**, **Küster, K.**, **Wagner, T.** and **Kasten, S.** (2008) Redox sensitivity of P cycling during marine black shale formation: dynamics of sulfidic

and anoxic, non-sulfidic bottom waters. *Geochim. Cosmochim. Acta*, **72**, 3703–3717.

McFadden, K. (2008) Integrated High-resolution Stratigraphy of the Doushantuo Formation, South China. PhD, Virginia Tech.

McFadden, K.A., **Huang, J.**, **Chu, X.**, **Jiang, G.**, **Kaufman, A.J.**, **Zhou, C.**, **Yuan, X.** and **Xiao, S.** (2008) Pulsed oxidation and biological evolution in the Ediacaran Doushantuo Formation. *Proc. Natl Acad. Sci.*, **105**, 3197–3202.

McLennan, S.M. (2001) Relationships between the trace element composition of sedimentary rocks and upper continental crust. *Geochem. Geophys. Geosyst.* **2**, 2000GC000109.

Meyer, K.M. and **Kump, L.R.** (2008) Oceanic euxinia in earth history: causes and consequences. *Annu. Rev. Earth Planet. Sci.*, **36**, 251–288.

Meyers, P.A., **Bernasconi, S.M.** and **Yum, J.-G.** (2009) 20 My of nitrogen fixation during deposition of mid-Cretaceous black shales on the Demerara Rise, equatorial Atlantic Ocean. *Org. Geochem.*, **40**, 158–166.

Mills, D.B., **Ward, L.M.**, **Jones, C.**, **Sweeten, B.**, **Forth, M.**, **Treusch, A.H.** and **Canfield, D.E.** (2014) Oxygen requirements of the earliest animals. *Proc. Natl Acad. Sci.*, **111**, 4168–4172.

Morford, J.L. and **Emerson, S.** (1999) The geochemistry of redox sensitive trace metals in sediments. *Geochim. Cosmochim. Acta*, **63**, 1735–1750.

Och, L.M. (2011) Biogeochemical cycling through the Neoproterozoic – Cambrian transition in China: an integrated study of redox-sensitive elements. PhD, University College London.

Och, L.M. and **Shields-Zhou, G.A.** (2012) The Neoproterozoic oxygenation event: environmental perturbations and biogeochemical cycling. *Earth-Sci. Rev.*, **110**, 26–57.

Och, L.M., **Shields-Zhou, G.A.**, **Poulton, S.W.**, **Manning, C.**, **Thirlwall, M.F.**, **Li, D.**, **Chen, X.**, **Ling, H.**, **Osborn, T.** and **Cremonese, L.** (2013) Redox changes in Early Cambrian black shales at Xiaotan section, Yunnan Province, South China. *Precambrian Res.*, **225**, 166–189.

Ohno, T., **Komiya, T.**, **Ueno, Y.**, **Hirata, T.** and **Maruyama, S.** (2008) Determination of $^{88}Sr/^{86}Sr$ mass-dependent isotopic fractionation and radiogenic isotope variation of $^{87}Sr/^{86}Sr$ in the Neoproterozoic Doushantuo Formation. *Gondwana Res.*, **14**, 126–133.

Partin, C.A., **Bekker, A.**, **Planavsky, N.J.**, **Scott, C.T.**, **Gill, B.C.**, **Li, C.**, **Podkovyrov, V.**, **Maslov, A.**, **Konhauser, K.O.**, **Lalonde, S.V.**, **Love, G.D.**, **Poulton, S.W.** and **Lyons, T.W.** (2013) Large-scale fluctuations in Precambrian atmospheric and oceanic oxygen levels from the record of U in shales. *Earth Planet. Sci. Lett.*, **369–370**, 284–293.

Piper, D.Z. (1994) Seawater as the source of minor elements in black shales, phosphorites and other sedimentary rocks. *Chem. Geol.*, **114**, 95–114.

Planavsky, N.J., **Rouxel, O.J.**, **Bekker, A.**, **Lalonde, S.V.**, **Konhauser, K.O.**, **Reinhard, C.T.** and **Lyons, T.W.** (2010) The evolution of the marine phosphate reservoir. *Nature*, **467**, 1088–1090.

Poulson Brucker, R.L., **McManus, J.** and **Poulton, S.W.** (2012) Molybdenum isotope fractionations observed under anoxic experimental conditions. *Geochem. J.*, **46**, 201–209.

Poulton, S.W. and **Canfield, D.E.** (2005) Development of a sequential extraction procedure for iron: implications for iron partitioning in continentally derived particulates. *Chem. Geol.*, **214**, 209–221.

Poulton, S.W. and **Canfield, D.E.** (2011) Ferruginous conditions: a dominant feature of the ocean through earth's history. *Elements*, **7**, 107–112.

Poulton, S.W. and **Raiswell, R.** (2002) The low-temperature geochemical cycle of iron: from continental fluxes to marine sediment deposition. *Am. J. Sci.*, **302**, 774–805.

Poulton, S.W., **Fralick, P.W.** and **Canfield, D.E.** (2004) The transition to a sulphidic ocean ~1.84 billion years ago. *Nature*, **431**, 173–177.

Poulton, S.W., **Fralick, P.W.** and **Canfield, D.E.** (2010) Spatial variability in oceanic redox structure 1.8 billion years ago. *Nat. Geosci.*, **3**, 486–490.

Qian, Z., **Zhensheng, D.** and **Xinzhi, Z**. (1995) Geochemical characteristics of Baiguoyuan black shale-type Ag-V deposit in Western Hubei Province. *Acta Mineral. Sinica*, **2**.

Quan, T.M. and **Falkowski, P.G.** (2009) Redox control of N: P ratios in aquatic ecosystems. *Geobiology*, **7**, 124–139.

Quan, T.M., **van de Schootbrugge, B.**, **Field, M.P.**, **Rosenthal, Y.** and **Falkowski, P.G**. (2008) Nitrogen isotope and trace metal analyses from the Mingolsheim core (Germany): evidence for redox variations across the Triassic-Jurassic boundary. *Global Biogeochem. Cycles*, **22**

Quan, T.M., **Wright, J.D.** and **Falkowski, P.G.** (2013) Co-variation of nitrogen isotopes and redox states through glacial-interglacial cycles in the Black Sea. *Geochim. Cosmochim. Acta*, **112**, 305–320.

Raiswell, R. and **Canfield, D.E.** (1996) Rates of reaction between silicate iron and dissolved sulfide in Peru Margin sediments. *Geochim. Cosmochim. Acta* **60**, 2777–2787.

Raiswell, R. and **Canfield, D.E.** (1998) Sources of iron for pyrite formation in marine sediments. *Am. J. Sci.*, **298**, 219–245.

Raiswell, R., **Newton, R.** and **Wignall, P.B.** (2001) An indicator of water-column anoxia: resolution of biofacies variations in the Kimmeridge Clay (Upper Jurassic, U.K.). *J. Sed. Res.*, **71**, 286–294.

Reddy, S.M. and **Evans, D.A.D.** (2009) Palaeoproterozoic supercontinents and global evolution: correlations from core to atmosphere. *Geol. Soc. Lond. Spec. Publ.* **323**, 1–26.

Reinhard, C.T., **Raiswell, R.**, **Scott, C.**, **Anbar, A.D.** and **Lyons, T.W.** (2009) A Late Archean sulfidic sea stimulated by early oxidative weathering of the continents. *Science*, **326**, 713–716.

Sahoo, S.K., **Planavsky, N.J.**, **Kendall, B.**, **Wang, X.**, **Shi, X.**, **Scott, C.**, **Anbar, A.D.**, **Lyons, T.W.** and **Jiang, G.** (2012) Ocean oxygenation in the wake of the Marinoan glaciation. *Nature*, **489**, 546–549.

Sarkar, A., **Chakraborty, P.P.**, **Mishra, B.**, **Bera, M.K.**, **Sanyal, P.** and **Paul, S.** (2010) Mesoproterozoic sulphidic ocean, delayed oxygenation and evolution of early life: sulphur isotope clues from Indian Proterozoic basins. *Geol. Mag.*, **147**, 206–218.

Scott, C.T., **Bekker, A.**, **Reinhard, C.T.**, **Schnetger, B.**, **KrapeÅ, B.**, **Rumble, D.** and **Lyons, T.W.** (2011) Late Archean euxinic conditions before the rise of atmospheric oxygen. *Geology* **39**, 119–122.

Scott, C., **Lyons, T.W.**, **Bekker, A.**, **Shen, Y.**, **Poulton, S.W.**, **Chu, X.** and **Anbar, A.D.** (2008) Tracing the stepwise oxigenation of the Proterozoic ocean. *Nature*, **452**, 456–460.

Shen, Y. and **Buick, R.** (2004) The antiquity of microbial sulfate reduction. *Earth Sci. Rev.*, **64**, 243–272.

Shen, Y., **Buick, R.** and **Canfield, D.E.** (2001) Isotopic evidence for microbial sulphate reduction in the early Archaean era. *Nature*, **410**, 77–81.

Shen, Y., **Canfield, D.E.** and **Knoll, A.H.** (2002) Middle Proterozoic ocean chemistry: evidence from the McArthur Basin, northern Australia. *Am. J. Sci.*, **302**, 81–109.

Shen, Y., **Knoll, A.H.** and **Walter, M.R.** (2003) Evidence for low sulphate and anoxia in a mid-Proterozoic marine basin. *Nature*, **423**, 632–635.

Shields, G.A., **Strauss, H.**, **Howe, S.S.** and **Siegmund, H.** (1999) Sulphur isotope compositions of sedimentary phosphorites from the basal Cambrian of China: implications for Neoproterozoic-Cambrian biogeochemical cycling. *J. Geol. Soc.*, **156**, 943–955.

Shields-Zhou, G. and **Och, L.** (2011) The case for a Neoproterozoic oxygenation event: geochemical evidence and biological consequences. *GSA Today*, **21**, 4–11.

Sigman, D.M., **Karsh, K.L.** and **Casciotti, K.L.** (2009) Nitrogen isotopes in the ocean. In: *Encyclopedia of Ocean Sciences* (Eds J.H. Steele, K.K. Turekian and S.A. Thorpe), pp. 40–54. Academic Press, Oxford.

Steiner, M. (1994) Die Neoproterozoischen Megaalgen Südchinas. *Berl. Geowiss. Abh.*, **15**, 1–146.

Steiner, M., **Li, G.**, **Qian, Y.**, **Zhu, M.** and **Erdtmann, B.-D.** (2007) Neoproterozoic to Early Cambrian small shelly fossil assemblages and a revised biostratigraphic correlation of the Yangtze Platform (China). *Palaeogeogr. Palaeoclimatol. Palaeoecol.*, **254**, 67–99.

Steiner, M., **Wallis, E.**, **Erdtmann, B.-D.**, **Zhao, Y.** and **Yang, R.** (2001) Submarine-hydrothermal exhalative ore layers in black shales from South China and associated fossils – insights into a Lower Cambrian facies and bio-evolution. *Palaeogeogr. Palaeoclim. Palaeoecol.*, **169**, 165–191.

Stiefel, E. (1997) Chemical keys to molybdenum enzymes*. *J. Chem. Soc., Dalton Trans.*, **1997**, 3915–3924.

Strauss, H. (2004) 4 Ga of seawater evolution: evidence from the sulfur isotopic composition of sulfate. *Geol. Soc. Am. Spec. Pap.*, **379**, 195–205.

Struck, U. (2012) On the use of stable nitrogen isotopes in present and past anoxic environments. In: *Anoxia* (Eds A.V. Altenbach, J.M. Bernhard and J. Seckbach), Vol. 21, pp. 497–513. Springer, The Netherlands.

Tribovillard, N., **Riboulleau, A.**, **Lyons, T.** and **Baudin, F.** (2004) Enhanced trapping of molybdenum by sulfurized marine organic matter of marine origin in Mesozoic limestones and shales. *Chem. Geol.*, **213**, 385–401.

Tribovillard, N., **Algeo, T.J.**, **Lyons, T.** and **Riboulleau, A.** (2006) Trace metals as paleoredox and paleoproductivity proxies: an update. *Chem. Geol.*, **232**, 12–32.

Vernhet, E. (2007) Paleobathymetric influence on the development of the late Ediacaran Yangtze platform (Hubei, Hunan, and Guizhou provinces, China). *Sed. Geol.*, **197**, 29–46.

Vernhet, E. and **Reijmer, J.J.G.** (2010) Sedimentary evolution of the Ediacaran Yangtze platform shelf (Hubei and Hunan provinces, Central China). *Sed. Geol.*, **225**, 99–115.

Vorlicek, T.P., **Kahn, M.D.**, **Kasuya, Y.** and **Helz, G.R.** (2004) Capture of molybdenum in pyrite-forming sediments: role of ligand-induced reduction by polysulfides. *Geochim. Cosmochim. Acta*, **68**, 547–556.

Wallis, E. (2006) The climatic and environmental history of the south Chinese Yangtze platform during the Neoproterozoic and early Cambrian: hydrothermally active and salinity stratified epicontinental basins, a key for understanding the „Cambrian Explosion"? Dr. rer. nat. Doctoral Thesis, TU Berlin.

Wang, J. and **Li, Z.X.** (2003) History of Neoproterozoic rift basins in South China: implications for Rodinia break-up. *Precambrian Res.*, **122**, 141–158.

Wang, X.F., **Erdtmann, B.-D.**, **Chen, X.H.** and **Mao, X.D.** (1998) Integrated sequence-, bio- and chemostratigraphy of the terminal Proterozoic to Lowermost Cambrian "black rock series" from central South China. *Episodes*, **21**, 12.

Wanty, R.B. and **Goldhaber, M.B.** (1992) Thermodynamics and kinetics of reactions involving vanadium in natural systems: accumulation of vanadium in sedimentary rocks. *Geochim. Cosmochim. Acta*, **56**, 1471–1483.

Wehrli, B. and **Stumm, W.** (1989) Vanadyl in natural waters: adsorption and hydrolysis promote oxygenation. *Geochim. Cosmochim. Acta*, **53**, 69–77.

Xiao, S. (2004) New multicellular algal fossils and acritarchs in Doushantuo chert nodules (Neoproterozoic; Yangtze Gorges, South China). *J. Paleontol.*, **78**, 393–401.

Xiao, S. and **Knoll, A.H.** (2000) Phosphatized animal embryos from the Neoproterozoic Doushantuo Formation at Weng'an, Guizhou, South China. *J. Paleontol.*, **74**, 767–788.

Xiao, S., **Zhang, Y.** and **Knoll, A.H.** (1998) Three-dimensional preservation of algae and animal embryos in a Neoproterozoic phosphorite. *Nature*, **391**, 553–558.

Yang, J.-D., **Sun, W.-G.**, **Wang, Z.-Z.** and **Wang, Y.-X.** (1996) Sm-Nd isotopic age of Precambrian-Cambrian boundary in China. *Geol. Mag.*, **133**, 53–61.

Yin, L., **Zhu, M.**, **Knoll, A.H.**, **Yuan, X.**, **Zhang, J.** and **Hu, J.** (2007) Doushantuo embryos preserved inside diapause egg cysts. *Nature*, **446**, 661–663.

Zerkle, A.L., **House, C.H.**, **Cox, R.P.** and **Canfield, D.E.** (2006) Metal limitation of cyanobacterial N_2 fixation and implications for the Precambrian nitrogen cycle. *Geobiology*, **4**, 285–297.

Zhang, Y., **Yin, L.**, **Xiao, S.** and **Knoll, A.** (1998) Permineralized fossils from the terminal Proterozoic Doushantuo Formation, south China. *Memoir (The Paleontological Society)*, **50**, 1–52.

Zhang, X., **Sigman, D.M.**, **Morel, F.M.M.** and **Kraepiel, A.M.L.** (2014) Nitrogen isotope fractionation by alternative nitrogenases and past ocean anoxia. *Proc. Natl Acad. Sci.*, **111**, 4782–4787.

Zhao, Z., **Xing, Y.**, **Ding, Q.**, **Liu, G.**, **Zhao, Y.**, **Zhang, S.**, **Meng, X.**, **Yin, C.**, **Ning, B.** and **Han, H.P.** (1988) *The Sinian System of Hubei*. China University of Geosciences Press, Wuhan.

Zhou, C. and **Xiao, S.** (2007) Ediacaran $\delta^{13}C$ chemostratigraphy of South China. *Chem. Geol.*, **237**, 89–108.

Zhou, C., **Tucker, R.**, **Xiao, S.**, **Peng, Z.**, **Yuan, X.** and **Chen, Z.** (2004) New constraints on the ages of Neoproterozoic glaciations in south China. *Geology*, **32**, 437–440.

Zhou, C., **Xie, G.**, **McFadden, K.A.**, **Xiao, S.** and **Yuan, X.** (2007) The diversification and extinction of Doushantuo-Pertatataka acritarchs in South China: causes and biostratigraphic significance. *Geol. J.*, **42**, 229–262.

Zhu, M.Y., **Zhang, J.M.**, **Steiner, M.**, **Yang, A.**, **Li, G.** and **Erdtmann, B.-D.** (2003) Sinian-Cambrian stratigraphic framework for shallow- to deep-water environments of the Yangtse platform: an intergrated approach. *Prog. Nat. Sci.*, **13**, 951–960.

Zhu, M., **Zhang, J.** and **Yang, A.** (2007) Integrated Ediacaran (Sinian) chronostratigraphy of South China. *Palaeogeogr. Palaeoclimatol. Palaeoecol.*, **254**, 7–61.

Zhu, M., **Lu, M.**, **Zhang, J.**, **Zhao, F.**, **Li, G.**, **Aihua, Y.**, **Zhao, X.** and **Zhao, M.** (2013) Carbon isotope chemostratigraphy and sedimentary facies evolution of the Ediacaran Doushantuo Formation in western Hubei, South China. *Precambrian Res.*, **225**, 7–28.

Zhuang, H., **Lu, J.**, **Fu, J.**, **Liu, J.**, **Ren, C.** and **Zou, D.** (1999) Evidence for transforming mineralization of Baiguoyuan silver-vanadium deposit hosted in black shale in Hubei, China. *Chin. Sci. Bull.*, **44**, 263–267.

Manuscript received 12 October 2014; revision accepted 27 May 2015

Supporting Information

Additional Supporting Information may be found in the online version of this article:

Table S1. Elemental and isotopic data.
Table S2. Iron Speciation.
Table S3. Xiaotan section, Yunnan Province (see Och et al., 2013 for more details).